An OSMR-CLIC1 cross talk drives key oncogenic pathways in glioblastoma

Amir Hossein Mansourabadi[1,2,3,*], Dianbo Qu[1,2,3*], Francesca Cianci[4*] Jamie Snider[5,#], Kamaldeep Randhawa[1,2,3, #], Laura Raco[1,2,3,6#], Max Kotlyar[7], Mohammad Al Ayach[1,2,3], Guido Rey[4], Shridhar Sanghvi[8], Mark Abovsky[7], Harpreet Singh[8], Artee H. Luchman[9], Dylan Burger[1,10], Janusz Rak[11], Vahab D. Soleimani[12], Igor Jurisica[7,13,14], Igor Stagljar[5,15,16,17,¶], Michele Mazzanti[4,¶] Arezu Jahani-Asl[1,2,3,7,18,19¶]

[1]Department of Cellular and Molecular Medicine, Faculty of Medicine, University of Ottawa, 451 Smyth Road, K1H 8M5, Ottawa, Canada
[2]University of Ottawa Brain and Mind Research Institute, 451 Smyth Road, K1H 8M5, Ottawa, Canada
[3]Ottawa Institute of Systems Biology, 451 Smyth Road K1H 8M5, Ottawa, Canada
[4]Laboratory of Cellular and Molecular Physiology, Department of Biosciences, University of Milano, Via Celoria 26, I-20133, Milano, Italy
[5]Donnelly Centre, University of Toronto, Ontario, Canada
[6]Division of Clinical and Translational Research, McGill University, 1001 Decarie Boulevard Montreal (Quebec) H4A 3J1
[7]Osteoarthritis Research Program, Division of Orthopedic Surgery, Schroeder Arthritis Institute, and Data Science Discovery Centre for Chronic Diseases, Krembil Research Institute, University Health Network, 60 Leonard Avenue, 5KD-407, Toronto, Ontario, Canada M5T 0S8
[8]Department of Physiology and Cell Biology, College of Medicine, The Ohio State University Wexner Medical Center, Columbus OH 43210
[9]Department of Cell Biology and Anatomy, Arnie Charbonneau Cancer Institute | Hotchkiss Brain Institute, Cumming School of Medicine, University of Calgary, AB, T2N 4N1
[10]Kidney Research Centre, Inflammation & Chronic Disease Program, Ottawa Hospital Research Institute, Ottawa, ON, K1H 8L6, Canada.
[11]Department of Pediatrics, Faculty of Medicine and Health Sciences, McGill University
[12]Department of Biochemistry, Microbiology and Immunology, Faculty of Medicine, University of Ottawa, 451 Smyth Road K1H 8M5, Ottawa, Canada
[13]Departments of Medical Biophysics and Computer Science, and Faculty of Dentistry, University of Toronto
[14]Institute of Neuroimmunology, Slovak Academy of Sciences, Bratislava, Slovakia
[15]Mediterranean Institute for Life Sciences, Meštrovićevo Šetalište 45, HR-21000 Split, Croatia
[16]Department of Biochemistry, University of Toronto, Ontario, Canada
[17]Department of Molecular Genetics, University of Toronto, Ontario, Canada
[18]Regenerative Medicine Program and Cancer Therapeutics Program, Ottawa Hospital Research Institute, Ottawa, ON, K1H 8L6, Canada.
[19]Gerald Bronfman Department of Oncology, McGill University, 5100 de Maisonneuve Blvd. West, Montréal, QC, H4A 3T2, Canada.
[*] And [#] Authors contributed equally
¶Correspondence: igor.stagljar@utoronto.ca, michele.mazzanti@unimi.it, arezu.jahani@uottawa.ca

Abstract

Oncostatin M receptor (OSMR) plays diverse and important roles in several human malignancies, including brain, breast, and pancreatic cancer.[1-4] Glioblastoma (GB) is the most malignant genetically diverse brain tumour, with no cure. The most common genetic mutation in GB is a truncated active mutant of epidermal growth factor receptor (EGFR), the EGFRvIII. OSMR orchestrates a feedforward signaling mechanism with EGFRvIII and the signal transducer and activator of transcription 3 (STAT3), to drive GB progression.[4] Beyond EGFRvIII, OSMR promotes brain tumour stem cells (BTSCs) via upregulation of mitochondrial oxidative phosphorylation and contributes to therapy resistance.[5] The molecular mechanisms underlying the multifaceted roles of OSMR in different contexts are largely unclear. Here, we systematically mapped the OSMR interactome using Mammalian Membrane Two-Hybrid High-Throughput Screening (MaMTH-HTS). This unbiased approach led to the identification of OSMR-specific and OSMR/EGFRvIII-specific binding proteins, revealing context-dependent OSMR functions. Among a subset of common interactors, we uncovered chloride intracellular channel 1 (CLIC1) as a critical regulator of both OSMR-STAT3 signaling and the OSMR/EGFRvIII complex in GB. CLIC1 physically associates with both OSMR and EGFRvIII and plays a key role in EGFRvIII packaging into extracellular vesicles (EVs). Genetic deletion of CLIC1 disrupts the OSMR/EGFRvIII interaction, impairs STAT3 activation, reduces EGFRvIII EV content, and slows GB progression. Using whole-cell patch-clamp recordings and a monoclonal antibody that selectively targets transmembrane CLIC1 (tmCLIC1omab), we establish a distinct pharmacologically and biophysically tmCLIC-mediated current in GB indispensable for sustaining EGFRvIII/STAT3 signaling. Importantly, we show that OSMR is required for maintaining CLIC1-mediated ionic balance at the plasma membrane (PM). Our study uncovers a bidirectional crosstalk

67 between OSMR and tmCLIC1 in GB, essential for fueling its malignant growth, and suggest that
68 disrupting the OSMR/tmCLIC1 interaction provides a promising therapeutic avenue for GB
69 treatment.

70 **Introduction**

71 GB is the most aggressive incurable brain tumour with a diverse genetic profile. The
72 oncogenic EGFRvIII mutant is present in more than 30% of GB patients and is initially assigned
73 to the classical GB subtype. The mesenchymal GB subtype has also been described as one of the
74 most malignant brain tumours. The aggressive nature of classical and mesenchymal subtypes is
75 attributed in large part to the activity of STAT3, endowing the cells with the ability to enter an
76 epithelial-to-mesenchymal (EMT)-like state, maintain stemness, grow, and metastasize.[6-9] Recent
77 studies have revealed that the cytokine receptor, OSMR, is a central player in propelling classical
78 and mesenchymal GB subtypes. OSMR plays a crucial role in mediating oncogenic signal
79 transduction initiated by the ligand OSM.[1,10] The OSM-OSMR induces the activation of STAT3
80 as well as key oncogenic pathways including the phosphoinositide 3-kinase (PI3K)–AKT, c-Jun
81 N-terminal kinases/mitogen-activated protein kinase (JNK/MAPK), and RAS/MAPK pathways.[11-
82 13] OSMR functions as a co-receptor for EGFRvIII in GB, inducing a positive feedback loop with
83 STAT3.[4] It also plays a crucial role in upregulating mitochondrial respiration, and conferring
84 resistance to ionizing radiation (IR) therapy.[5] Additionally, OSMR is a key regulator of brain
85 tumour stem cell (BTSC) self-renewal[5] and the immune microenvironment[14], suggesting that its
86 function is highly context-dependent.

87 Here, we employed MaMTH-HTS, a technology uniquely suited to identifying interacting
88 partners of integral membrane proteins. Our screening revealed that OSMR physically and
89 functionally interacts with tmCLIC1, positioning it as a central player in both OSM/OSMR

90 cytokine signaling and the OSMR/EGFRvIII co-receptor complex. We demonstrate that the
91 genetic deletion of tmCLIC1 and pharmacological inhibition of tmCLIC1 impairs BTSCs, and
92 oncogenic EGFRvIII/STAT3 signaling. Furthermore, our data show that OSMR is essential for
93 the function of the membrane configuration of CLIC1, highlighting a previously unrecognized
94 crosstalk between a cytokine receptor and an ion channel in driving key oncogenic pathways in
95 GB. Our finding has important implications for the design of novel therapeutic strategies to
96 suppress GB.
97

98 **Results**

99 **Mapping OSMR interactome via Mammalian Membrane Two-Hybrid High Throughput**
100 **Screening (MaMTH-HTS)**

101 To address the question of how OSMR networks with alternate molecules to confer its
102 different functions, we performed MaMTH-HTS in HEK293T cells expressing OSMR bait, in the
103 presence or absence of co-expressed EGFRvIII, alongside a prey library of ~8000 open reading
104 frames from the Human ORFeome V8.1 collection (**Supp Fig. 1a-c**).[15] We identified 334 high-
105 confidence candidate binding partners for OSMR (**Fig. 1**), following rigorous analyses and
106 exclusion of MaMTH-HTS 'frequent flyers', which was established from repeated MaMTH-HTS
107 results of 9 'individual bait' protein control experiments, as previously described.[16] Among the
108 identified candidates, 204 hits, including 59 PM proteins, were detected when OSMR was used as
109 bait in the absence of EGFRvIII, and 160 candidate binding partners, including 40 PM proteins,
110 were identified when OSMR was used as a bait in the presence of EGFRvIII. Importantly, our data
111 revealed 30 candidate binding partners of OSMR that were commonly shared by both groups, 7 of
112 which were PM proteins. The PM proteins encompassed proteins that are integral to the membrane

113 as well as proteins that are associated with the membrane. GO term functional analysis of protein
114 clusters in each group revealed molecules engaged in metabolic processes and signalling as top
115 categories underscored in each group (**Fig. 1**). Furthermore, these analyses revealed that the GO
116 term for immune system processes was highly enriched in OSMR-unique interactome, whereas
117 the regulation of biogenesis processes was among top GO terms for OSMR-EGFRvIII category.
118 This novel OSMR interactome map highlights its role in different biological processes with unique
119 variations depending on a cell's genetic signature.
120

121 **Analysis of OSMR common binding partner and the involvement of CLIC1**

122 To unravel the mechanism by which OSMR operates to promote tumour growth across
123 different GB subtypes, we focused on the common candidate binding partners (**Supp. Table 1**),
124 which encompassed different classes of proteins including metabolic processes, signalling,
125 biogenesis, development, and immune system processes. To validate MaMTH data in the context
126 of GB, we employed four different patient-derived BTSCs that naturally harbour EGFRvIII
127 mutation (BTSC73 and BTSC147) or lack the mutation (BTSC12, BTSC30) (**Supp. Table 2**). We
128 conducted a counter-screen in which we employed siRNA (**Supp. Table 3**) targeting each of the
129 genes encoding these proteins, followed by assessing cell viability. Our results revealed that
130 knockdown (KD) of 12 genes demonstrated a substantial reduction in cell viability exceeding 50%
131 across different BTSCs (**Supp. Fig. 1d**). These included *CLEC2B*, *CLIC1*, *CREB3*,
132 *CSGALNACT2*, *DCN*, *EIF2C3*, *GC*, *GPBP1*, *H3C1*, *IMMP2L*, *NAT8*, and *ST3GAL4*. Prior to
133 follow up investigation on select candidates, we applied additional screening criteria pertaining to
134 the known role of these proteins in BTSCs and GB as well as their known roles in regulation of
135 different hallmarks of cancer. These criteria led us to focus on CLIC1, as the top candidate.

136 CLIC1 is highly expressed in various cancers including GB, with its expression
137 significantly correlating with poor prognosis.[17] CLIC1 exists as a soluble cytoplasmic protein,
138 however, under specific cellular conditions that are favored in cancer cells[18], it can translocate to
139 PM where it functions as an ion channel.[19,20] Interestingly, similar to OSMR[13], CLIC1 is highly
140 expressed in the mesenchymal GB subtype and enriched in cancer stem cells (CSCs)[17], where it
141 promotes proliferation.[21] We conducted analysis of four publicly available patient datasets
142 deposited in TCGA, Rembrandt, Gravendeel, Kamoun, and assessed the mRNA expression of
143 CLIC1 and OSMR in GB tumour versus non- tumour samples. Both OSMR and CLIC1 were
144 consistently upregulated in GB samples, across TCGA, Rembrandt, and Gravendeel datasets (**Fig.**
145 **2a,b**). Importantly, CLIC1 and OSMR expression analysis across different GB subtypes revealed
146 that CLIC1 displays consistent and significant upregulation with subtype progression while OSMR
147 was equally upregulated in both classical and mesenchymal subtypes relative to proneural subtype
148 **(Fig. 2c,d**). Next, we analyzed how upregulation of OSMR and CLIC1 impacts GB patient
149 survival. Analysis of 4 independent datasets deposited at TCGA, Rembrandt, Gravendeel and
150 LeeY revealed that patients with high expression of CLIC1 or OSMR had the worst prognosis
151 (**Supp. Fig. 2a-h**). Importantly, patients stratified as CLIC1/OSMR high expressors had
152 significantly shorter lifespan compared to CLIC1/OSMR low expressors (**Fig. 2e-h**). Our data
153 suggest that stratification of patients for CLIC1 and OSMR expression is an important predictor
154 of survival.
155
156 **CLIC1 Regulation of BTSCs self-renewal and proliferation**
157 To characterize the impact of CLIC1 knockdown on a panel of patient-derived BTSC with varying
158 oncogenic mutations, we next electroporated a pool of four siRNAs targeting CLIC1 into different

159 BTSCs and assessed cell viability and stem cell frequency using PrestoBlue and extreme limiting
160 dilution assay (ELDA)[22], respectively. RT-qPCR and immunoblotting analyses showed efficient
161 siRNA-mediated knockdown of CLIC1 by greater than 85% and a significant decline in CLIC1
162 protein expression level relative to BTSCs electroporated with a non-targeting RNAi (siCTL) (**Fig.**
163 **3a-d, Supp. Fig. 3a-j**). Our data revealed a significant decrease in BTSC viability (**Supp. Fig.**
164 **3k,l**), BTSC sphere size (**Supp. Fig. 3m,n**), and stem cell frequency (**Fig. 3e-h**) upon KD of
165 CLIC1. Next, we generated BTSCs in which we induced genetic deletion of CLIC1 using CRISPR
166 in two different EGFRvIII-expressing BTSC73 and BTSC147 (**Fig. 3i-l**). Similar to our findings
167 with the transient KD experiments, monoallelic (CRISPR-m) or biallelic (CRISPR-b) genetic
168 deletion of CLIC1 induced a robust reduction in BTSC stem cell frequency (**Fig. 3m,n**), cell
169 viability (**Supp. Fig. 3o,p**), and sphere size (**Supp. Fig. 3q,r**). We next conducted EdU assay.
170 Consistent with our results, deletion of CLIC1 resulted in a significant reduction in actively
171 dividing cells (**Fig. 3o,p, Supp. Fig. 4**). Taken together, our data confirm that CLIC1 is essential
172 for maintaining cell viability, stem cell self-renewal and proliferation of BTSCs derived from
173 glioblastoma patients.
174
175 **CLIC1 interacts with OSMR and EGFRvIII endogenously in BTSCs**
176 MaMTH data revealed that CLIC1 is a high confidence potential binding partner of OSMR.
177 We first subjected different non-permeabilized BTSCs to immunostaining using an antibody to
178 CLIC1 and observed localization of CLIC1 at the cell periphery (**Fig. 4a-c**). To assess whether
179 CLIC1 and OSMR colocalize in BTSCs, we conducted co-immunostaining using antibodies to
180 OSMR and CLIC1. Our data revealed that CLIC1 colocalizes with OSMR in all the BTSCs
181 analyzed in our studies (**Fig. 4d-g**), raising the question of whether CLIC1 interacts with OSMR

182 endogenously. We conducted Proximity Ligation Assay (PLA) using OSMR and CLIC1
183 antibodies in different BTSCs and used BTSCs subjected to PLA with primary antibodies omitted
184 as control. Our data showed *in situ* interaction of CLIC1 with OSMR across all BTSC lines that
185 were examined (**Fig. 4h-l**), with EGFRvIII-expressing BTSC 73 and 147 that harbour elevated
186 OSMR expression, exhibiting stronger signal (**Fig. 4h,i, l**) compared to BTSCs 30 and 12 lacking
187 the EGFRvIII (**Fig. 4j,k, l**). To further confirm the specificity of the interaction signal, we
188 subjected CLIC1 CRISPR- BTSCs and their corresponding controls to PLA analysis. For each
189 BTSCs two CRISPR lines, CRISPR-m and CRISPR-b, were included. Our results showed that the
190 PLA interaction signal of OSMR-CLIC1 was robustly diminished in CLIC1 CRISPR BTSCs
191 compared to control BTSCs (**Fig. 4m-p**).

192 Next, we subjected the BTSCs to co-immunoprecipitation (co-IP) experiments using an
193 antibody against endogenous OSMR followed by immunoblotting with a CLIC1 antibody. Our
194 data showed that OSMR interacts with CLIC1 endogenously in BTSCs (**Fig. 4q,r**).

195 Given that OSMR forms a co-receptor with EGFRvIII, we next asked whether CLIC1 is a
196 component of the same complex with EGFRvIII. We conducted co-immunostaining analysis in
197 different BTSCs and found colocalization of EGFRvIII with CLIC1 (**Fig. 4s,t**). Thus, we
198 performed PLA experiments using antibodies to EGFRvIII and CLIC1 in control and CLIC1
199 CRISPR BTSCs. Our results showed *in situ* interaction of CLIC1 with EGFRvIII (**Fig. 4u,v**).

200

201 **The extracellular domain of CLIC1 interacts with OSMR/EGFRvIII**

202 OSMR is found in complex with EGFRvIII to amplify receptor tyrosine kinase (RTK)
203 signalling.[4] Given our results that CLIC1 interacts with both OSMR and EGFRvIII, we asked
204 whether CLIC1 is required for the OSMR/EGFRvIII interaction. We subjected CLIC1 CRISPR

205 and corresponding control BTSCs to PLA analysis using antibodies to OSMR and EGFRvIII.
206 Strikingly, genetic deletion of CLIC1 significantly impaired the interaction of OSMR with
207 EGFRvIII in each of BTSC147 and BTSC73 that harbour EGFRvIII mutation (**Fig. 5a-e**),
208 revealing that CLIC1 is required for OSMR/EGFRvIII complex. In parallel, we conducted similar
209 experiments in which we assessed CLIC1-OSMR interaction in EGFRvIII knockdown BTSCs and
210 EGFRvIII-CLIC1 interaction in OSMR knockdown BTSCs. Our results suggest that CLIC1 and
211 OSMR interact independently of EGFRvIII, although the presence of EGFRvIII generates stronger
212 interaction signal (**Supp. Fig. 5a**), most probably due to the fact that OSMR expression is
213 upregulated downstream of EGFRvIII-STAT3 signalling.[4]

214 Given that CLIC1 functions as a membrane protein existing predominantly as a
215 homodimer, we next modeled its interaction using the dimer of CLIC1(residues 1-24) extracellular
216 domain with the extracellular domains of OSMR (residues 1–741) and EGFRvIII (residues 1–378)
217 using AlphaFold-Multimer. The predicted structural model of this tetramer revealed that the
218 CLIC1 dimer (purple and brown) interacts with OSMR (green) and EGFRvIII (orange) (**Fig. 5f**).
219 Given that the extracellular region of CLIC1 comprises only 24 amino acids (aa), we included its
220 transmembrane domain (residues 25–58 aa) for binding assays. Consistent with the prediction, our
221 experiments using CLIC1(1–58 aa) and CLIC1(1–178 aa) as baits demonstrated that CLIC1(1–58
222 aa) interacts with OSMR or with the OSMR/EGFRvIII complex, indicating that the extracellular
223 regions of these three proteins are sufficient to support complex formation (**Fig. g,h**). To further
224 validate the interaction under native conditions, we performed native gel electrophoresis, which
225 preserves intact protein complexes. The results revealed that CLIC1, OSMR, and EGFRvIII
226 coexist within a ~720 kDa protein complex in EGFRvIII- expressing BTSCs (**Fig. 5i**).
227 Additionally, we confirmed that the protein expression of each of the molecules in the complex is

228 not altered by the presence of its binding partners as revealed via immunoblotting analysis in
229 BTSCs (**Supp Fig. 5b-d**), and IF staining on tumour tissues (**Supp Fig. 5e**). To investigate the
230 regulatory relationship between EGFRvIII and STAT3 in controlling CLIC1 expression, we used
231 EGFRvIII-expressing $STAT3^{loxp/loxp}$, $STAT3^{-/-}$, murine stem cell virus (MSCV)-CTL (non–
232 EGFRvIII-expressing) $STAT3^{loxp/loxp}$ and $STAT3^{-/-}$ astrocytes. No differences in CLIC1 expression
233 were observed among the groups, indicating that STAT3 does not regulate CLIC1 expression
234 (**Supp Fig. 5f**). Next, we asked if the complex formation is impacted by lipid rafts bringing these
235 molecules together. We treated BTSCs with Methyl-β-cyclodextrin (MβCD), to disrupt lipid rafts,
236 followed by PLA analysis. We observed a reduction in the interaction signal between CLIC1 and
237 OSMR suggesting that their interaction in part occurs within these lipid rafts on the plasma
238 membrane (**Supp Fig. 6**).
239
240 **OSMR-CLIC1 cross-talk maintain EGFRvIII/STAT3 signalling, and blockade of**
241 **transmembrane CLIC1 (tmCLIC1) impairs the phosphorylation of EGFRvIII and STAT3**
242 Our data raised the question of whether CLIC1 functionally regulates the oncogenic OSMR-
243 STAT3 and EGFRvIII signalling. CLIC1 is found as a soluble cytoplasmic protein as well as a
244 transmembrane protein that forms an ion channel.[21] We conducted cell fractionation experiments
245 in different BTSCs and found that CLIC1 is localized to both the membrane and cytoplasm (**Supp.**
246 **Fig. 7**), although, the majority of CLIC1 was found in the cytoplasm. CLIC1 is shown to be
247 packaged into extracellular vesicles (EVs) in order to target neighbouring cells[23], promoting
248 tumour growth.[23,24] Interestingly, similar to CLIC1[17,23,25], EGFRvIII impacts various aspects of
249 tumourigenesis not only in the cell of origin, but in the neighbouring cells, also shown to be
250 mediated via EVs.[26] Thus, we first questioned whether CLIC1 is required for the horizontal

251 propagation of EGFRvIII to the neighboring cells. By extracting EVs from CTL BTSCs and their
252 corresponding CLIC1 CRISPR cells, we evaluated EGFRvIII protein expression levels in the cell
253 lysates and EV fractions. Immunoblotting analysis revealed that EGFRvIII levels were
254 significantly reduced in CLIC-deleted EVs, suggesting a role for CLIC1 in mediating the
255 horizontal propagation of EGFRvIII to the neighboring cells (**Fig. 6a-c**, **Supp. Fig. 8)**. Next, we
256 set out to investigate the electrophysiological properties of tmCLIC1 in three distinct human BTSC
257 lines including BTSC73, BTSC147, and BTSC30. To assess basal level tmCLIC1 levels, we used
258 IAA94, a known blocker of CLIC1. The tmCLIC1 current was measured as the IAA94-sensitive
259 current, defined as the difference between the initial current and the current after drug perfusion.
260 We conducted an electrophysiological evaluation of tmCLIC1 levels at +40mV on the membranes
261 of CLIC1 CRISPR and control BTSCs. Our results revealed that the tmCLIC1 currents were
262 significantly reduced in the CLIC1 CRISPR lines compared to the CTL BTSCs (**Fig. 6d**). To assess
263 whether OSMR is required for the tmCLIC1 mediated ionic conductance, we induced KD of
264 OSMR using short hairpin RNA (shOSMR) in different cell lines and subjected the OSMR
265 knockdown (KD) and control (CTL) Scrambled (SCR) cells to patch clamp experiments to
266 evaluate whether reduced OSMR expression levels alter Cl^- currents. Cell currents were assessed
267 both prior to (baseline) and following the addition of 100 mM of CLIC1 inhibitor, IAA94 to the
268 bath solution (**Fig. 6e-j**). The tmCLIC1 current was measured as the IAA94-sensitive current,
269 defined as the difference between the initial current and the current after drug perfusion. The
270 corresponding current-voltage relationship was recorded in each group. Strikingly, our data
271 revealed that inhibition of OSMR significantly attenuated the tmCLIC1-associated Cl^- current
272 (**Fig. 6i-k).** Our data reveals a bidirectional OSMR-CLIC1 cross talk in regulation of CLIC1-
273 mediated ionic conductance in BTSCs, leading to the question of whether tmCLIC1 impacts

274 EGFRvIII/STAT3 signalling. To address this question, we generated and employed a monoclonal
275 CLIC1 antibody (tmCLIC1omab®) that specifically inhibits tmCLIC1 and its associated ionic
276 currents (**Fig. 6l-p**, **supp. Fig. 9a-d**). We first assessed the tmCLIC1 antibody in tumour assays in
277 which BTSCs xenografted in the flanks of SICD mice were treated with tmCLIC1 antibody or IgG
278 control. Strikingly, tmCLIC1 significantly suppressed tumour growth in the antibody treated group
279 (**Fig. 6q-s**). Next, we treated different glioma cells and BTSCs with the tmCLIC1omab or IgG
280 control, followed by an analysis of EGFRvIII and STAT3 phosphorylation in response to the
281 ligand OSM. Our data revealed that both the EGFR phosphorylation at tyrosine (Y) 1068 and
282 STAT3 phosphorylation at Y705 were significantly attenuated upon inhibition of the CLIC1-
283 mediated Cl- current by a tmCLIC1 antibody in EGFRvIII expressing BTSC 147 and 73.
284 Importantly, tmCLIC1omab® had no impact on EGFRvIII-STAT3 signalling in BTSC30 that
285 naturally does not harbour the EGFRvIII or elevated STAT3 expression (**Fig. 6t-y, Supp. Fig.**
286 **10**).
287 Taken together, we provide data that tmCLIC1 regulates OSM/OSMR-STAT3 and
288 OSMR/EGFRvIII oncogenic signalling and at the same time OSMR promotes tmCLIC1 function.
289 We establish that the cooperation of OSMR with tmCLIC1 is required to maintain key oncogenic
290 pathways in GB.
291

292 **CLIC1 drives GB tumourigenesis and maintains EGFRvIII/EGFR phosphorylation *in vivo***

293 Our findings on a central role of CLIC1 in regulation of OSMR/EGFRvIII interaction and
294 EGFRvIII and STAT3 phosphorylation led us next to examine whether CLIC1 contributes to GB
295 tumourigenesis *in vivo*. We conducted intracranial tumour assay using BTSC73, BTSC147, and
296 corresponding CLIC1 CRISPR BTSCs lines. Our data revealed that deletion of CLIC1

297 significantly impaired tumourigenesis, and prolonged survival (**Fig. 7a-h**). We next subjected
298 tumour sections obtained from the control mice as well as the smaller tumours from the CLIC1
299 CRISPR group to H&E staining (**Fig. 7i,j**) and immunostaining analysis using a phospho-Y1068-
300 EGFR antibody that can detect both the phosphorylated wild type (WT) EGFR and EGFRvIII (**Fig.**
301 **7k**). Strikingly, we found that the phosphorylation of EGFR/EGFRvIII was robustly attenuated in
302 the mice group xenografted with CLIC1 CRISPR BTSCs. Independently, we subjected different
303 CLIC1 CRISPR and control BTSCs to immunoblotting experiments and analyzed the
304 phosphorylation events using antibodies to STAT3-Y-705 and EGFRvIII. Strikingly, similar to
305 results obtained with tmCLIC1moab, we established that genetic deletion of CLIC1 significantly
306 impairs the phosphorylation of STAT3 and EGFRvIII. (**Fig. 7l-s**). Our data suggest that CLIC1
307 tightly maintains the activation of EGFRvIII and STAT3.
308

309 **Discussion**

310 In this study, we comprehensively mapped the OSMR interactome to identify its high
311 confidence binding partners under different conditions leading to a better understanding of
312 OSMR's multifaceted roles in GB progression. Through systematic protein-protein interaction
313 mapping using MaMTH-HTS, followed by counter-screening and loss- and gain-of-function
314 studies, we demonstrate that tmCLIC1 interacts with OSMR physically, independently of the
315 genetic background of the cells, and acts as a critical regulator of diverse oncogenic pathways
316 driven by OSMR, EGFRvIII, and STAT3. We demonstrate a bidirectional relationship for
317 tmCLIC1-OSMR interaction, which plays a pivotal role in regulating ion conductance, thereby
318 driving GB progression.

319 CLIC1 has been implicated in multiple malignancies, including lung cancer[27], pancreatic
320 adenocarcinoma[28], epithelial ovarian cancer[29], and medulloblastoma.[30] It is associated with poor
321 prognosis in GB and is abundantly expressed in CSCs.[17,31] Previous studies have highlighted the
322 role of tmCLIC1 in cellular proliferation and viability, with genetic deletion leading to cell
323 swelling, mitotic defects, and reduced proliferation in medulloblastoma cells.[30] tmCLIC1 may act
324 as a cell cycle accelerator by mediating cell volume changes. For instance, during the prophase to
325 metaphase transition, cells undergo a significant volume decrease, reaching a minimum size at
326 metaphase. This reduced volume is preferred by the cell and is referred to as pre-mitotic
327 condensation.[32,33] Pre-mitotic condensation requires the efflux of Cl-, which may be mediated by
328 tmCLIC1. tmCLIC1 has also been shown to play a prominent role in ROS production[18,34,35], and
329 cell cycle regulation.[36] For example, IAA94-mediated inhibition of tmCLIC1 is shown to prolong
330 the G1 phase, thereby extending the overall cell cycle duration.[37] In agreement with these findings,
331 our data show that CLIC1 deletion suppresses BTSC self-renewal and proliferation, suggesting its
332 role in cell cycle regulation. Given tmCLIC1's established function in maintaining redox balance[38],
333 its knockdown likely elevates oxidative stress and disrupts redox homeostasis, thereby impairing
334 BTSC proliferative capacity and self-renewal potential. These findings reinforce the idea that
335 CLIC1 is a critical regulator of GB cell division and tumour aggressiveness. The interplay between
336 ROS, tmCLIC1-generated chloride currents, combined with evidence of tmCLIC1/OSMR
337 interaction, highlights the need to investigate CLIC1's role in CSCs' metabolism in the context of
338 GB. Whether similar to OSMR[5], tmCLIC1 regulates oxidative phosphorylation (OXPHOS) to
339 maintain BTSCs and buffer ROS in the mitochondria remains to be investigated.

340 We further demonstrate a crucial role for CLIC1 in maintaining EGFRvIII intracellularly.
341 This effect may also be attributed to CLIC1's role in tumour microenvironment modulation, as it

342 is positively associated with stromal activation, epithelial-mesenchymal transition (EMT), and
343 angiogenesis, hallmarks of GB progression.[39] Chloride channels, including CLIC1, have been
344 implicated in innate and adaptive immune responses, particularly in phagocyte-mediated
345 immunity. CLIC1 is required for phagosomal acidification and antigen processing, which are
346 crucial for $CD4^+$ T cell activation.[39-41] CLIC1-mediated regulation of macrophage-driven
347 inflammation and ROS production may facilitate the establishment of a tumour-promoting
348 microenvironment conducive to tumour growth and metastasis. Furthermore, CLIC1 plays a role
349 in the innate immune system through its involvement in the activation of NLRP3 inflammasome.[42]
350 Aberrant activity of the NLRP3 inflammasome has been implicated in the progression of several
351 cancers including glioma.[43,44] Additionally, tmCLIC1 modulates Cl^- currents in activated
352 microglia, particularly in response to β-amyloid protein (Aβ) stimulation.[35] Interestingly, OSMR
353 and its ligand OSM operate in a paracrine fashion in which OSM secreted via immune cells
354 typically binds the receptor on the tumour cells to direct oncogenic signalling. These findings
355 suggest that OSMR-CLIC1 cross talk may influence immune surveillance, an area that requires
356 future investigation.

357 It is also possible that loss of CLIC1 induces a cell shift towards a more differentiated
358 phenotype. Previous research on cell fate dynamics supports this notion. Stockhausen et al.
359 demonstrated that induced differentiation of BTSCs with serum leads to loss of EGFRvIII
360 expression and decreased tumourigenic potential.[45] In another study by Gritti et al., CLIC1
361 expression was lost upon induction of differentiation with FBS.[46] These results suggest that both
362 EGFRvIII and CLIC1 are important in maintaining stemness. Similarly, in another study by He et
363 al., the chloride channel, Ano1, was found to limit the differentiation of epithelial progenitors
364 towards cells of the secretory lineage.[47] Further studies are required to determine if the interaction

365 of CLIC1 with EGFRvIII aids in establishing a cellular network that suppresses the BTSCs
366 differentiation.

367 In this study, we provide data showing that CLIC1 regulates the horizontal transfer of
368 EGFRvIII via EV. We observed a striking attenuation of EGFRvIII in EVs derived from CLIC1
369 CRISPR cells, suggesting that CLIC1 may regulate EGFRvIII packaging, thereby influencing
370 neighboring cells. In support of this model, tmCLIC1 vesicle transfer has been implicated in
371 glioma stem cell proliferation.[23] Furthermore, blocking of the chloride current in stem-like cells
372 through the re-purposing of known pharmacological drugs, suggests that tmCLIC1 could be a
373 promising target for therapy.[46,48] Similarly, tumour cells in GB are shown to impact neighboring
374 cells via transferring EGFRvIII through EV.[26] Another study in gastric cancer revealed that the
375 presence of CLIC1 in EVs is associated with resistance to vincristine by transferring resistance
376 traits to neighboring cells.[24] Whether tmCLIC1 functional expression represents an adaptive
377 mechanism enabling drug resistance in GB remains an exciting area of research to be explored.

378

379 Our findings have established that tmCLIC1 interaction with OSMR and EGFRvIII is
380 essential for sustaining oncogenic signaling. Using a monoclonal CLIC1 antibody that can only
381 target tmCLIC1, we establish the significance of tmCLIC1, however, the functional contribution
382 of cytoplasmic CLIC1 and its involvement in mitochondrial and metabolic pathways remains to
383 be investigated in GB.

384 In conclusion, our findings establish tmCLIC1 as a central player in GB pathogenesis,
385 orchestrating cytokine networks and enhancing the RTK signalling. Its interaction with OSMR
386 and EGFRvIII is critical for sustaining BTSC self-renewal and GB tumourigenesis. These results
387 highlight tmCLIC1 as a promising therapeutic target, suggesting that its inhibition, in combination

388 with standard GB treatments, may lead to improved patient outcomes. Importantly, our data
389 suggests that inhibiting the interaction of CLIC1 and OSMR in GB using small inhibitory peptides
390 serves as a promising therapeutic avenue for GB.
391

392 **Materials and methods**

393 **Brain tumour Stem Cell (BTSC) and generation of transgenic cell lines**

394 The human BTSC lines 73, 147, 12, and 30 were generously provided by Dr. Samuel Weiss at the
395 University of Calgary. They were generated in accordance with the University regulation from
396 excess or discarded tissue collected during surgery from adult patients following informed consent
397 from patients. BTSCs were characterised for major mutations (**Supp. Table 2**) and were cultured
398 and maintained, as described in Supplementary Materials and methods section. Transgenic
399 CRISPR BTSCs were generated, using methods previously described.[49] To design the gRNA, Off-
400 Spotter software, version 0.2.2 (https://cm.jefferson.edu/Off-Spotter/), was used. Two guide RNA
401 strands (forward and reverse complement) were generated to target exons 5-9 of the CLIC1 gene.
402 To generate the construct, the Golden Gate Assembly Cloning strategy[50] was used in which
403 gRNA1 and gRNA2 were cloned into pL-CRISPR.EFS.GFP (Addgene plasmid #57818), and pL-
404 CRISPR.EFS.tRFP (Addgene plasmid, #57819), plasmids, respectively. Plasmids were sequenced
405 (Genome Quebec), verified and electroporated [1300 volts by the AMAXA nucleofector 2b device
406 (Lonza, #AAB1001) to deliver 3 µg of each plasmid construct (gRNA1-GFP and gRNA2-RFP)
407 into ~2 million BTSC147 or BTSC73]. Electroporated cells were cultured in a T-75 low
408 attachment flask at 37°C in a 5% CO_2. 48 hours after electroporation, BTSC spheres were
409 dissociated into a single cell suspension using Accumax dissociation solution (Innovative Cell
410 Technologies, #AM105) and subjected to Fluorescent Activated Cell Sorting (FACS) analysis

411 using the BD FACSAriaTM Fusion (BD Biosciences) to sort for double positive GFP and RFP
412 cells. Sorted cells were plated at a density of 1 cell/well into two 96-well plates containing 100 µl
413 of BTSC media. Wells were monitored every two days to assess sphere formation and clonal
414 samples were collected from multiple positive clones and were subject to genomic DNA isolation.
415 Isolated DNA was analysed by PCR using internal primers and external primers to the gRNA-
416 guided CAS9 cut site, designed using Primer3Plus software, version 3.3.0
417 (https://www.primer3plus.com/), to determine monoallelic, biallelic, or non-deletion control
418 clones. Monoallelic deletion clones in both BTSC73 and BTSC147 cell lines were determined by
419 PCR in which the presence of one internal and one external band on a 2% Agarose gel, was
420 observed, while a biallelic deletion was determined by a single external band. Knockout or
421 knockdown of CLIC1 was validated using RT-qPCR and WB to assess gene and protein
422 expression. Since there we no clones identified that presented no cuts in the CLIC1 gene following
423 incubation with the CRISPR-CAS9 construct, which could have been used as a control for CAS9,
424 the chosen control for experiments using the CRISPR-CAS9-CLIC1 cells was that of the parental
425 BTSC73 or BTSC147 line. The gRNA and primer sequences used in this experiment are listed in
426 **Supp. Table 4**. Finally, short Interfering RNA (siRNA) was used to generate transient knockdown
427 (KD) in patient-derived BTSCs. BTSCs were processed into a single-cell suspension. ON
428 TARGET-plus SMART pool human CLIC1 siRNA (Dharmacon, #L-009530-00-0005) at a
429 concentration of 100 nM, and ON TARGET-plus non-targeting pool (Dharmacon, #D-001810-10-
430 05), were employed, as described in Supplemental Materials and methods section.
431
432 **Mammalian Membrane Two-Hybrid-High Throughput Screen (MaMTH-HTS)**

433 To identify binding partners of OSMR in the presence and absence of EGFRvIII,
434 Mammalian Membrane Two-Hybrid (MaMTH) High Throughput Screen (HTS) technology was
435 used as described.[16,51] Briefly, plasmid expressing OSMR 'Bait' protein with C- terminally fused
436 MaMTH-HTS Bait tag (Cub-GAL4TF-P2A-tagBFP) alone or alongside plasmid expressing
437 EGFRvIII (fused with 3xFLAG at its N-terminus) was transfected into a pooled 'Prey' library of
438 HEK293T MaMTH-HTS reporter cell lines. The library of reporter cell lines stably expressed
439 members of the Human ORFeome V8.1 collection (~8000 open reading frames - ORF's) fused to
440 MaMTH-HTS Prey tag (Nub) at their N-terminus and P2A-mCherry at their C-Terminus and
441 contained chromosomally integrated GFP reporter under the control of the GAL4 transcription
442 factor (GAL4TF) promoter. Transfections were performed using X-tremeGene™ 9 Transfection
443 Reagent (Roche, XTG9-RO) as specified by the manufacturer protocol. In order to induce Bait
444 (**Supp. Fig. 1**) and Prey expression, cells were grown for 2-3 days in the presence of 0.5 µg/ml
445 Tetracycline in the following conditions: 37°C, 5% CO_2 in DMEM containing 10% FBS, and 1%
446 Penicillin/Streptomycin media. Cells were then harvested by trypsinization and resuspended at a
447 concentration of 1-2 x 10^6 cell/ml in Basic Sorting Buffer (1X PBS, 5 mM EDTA, 25 mM HEPES
448 pH 7.0, 1% BSA) and subjected to sorting by Flow Cytometry using BD FACSMelody (BD
449 Biosciences). Cells were sequentially selected according to the following: tag-BFP fluorescence
450 indicating 'Bait' expression, mCherry fluorescence indicating 'Prey' expression, and GFP
451 fluorescence indicating Bait-Prey interaction. Cells were collected for analysis in DMEM
452 containing 25% FBS and centrifuged pellets were processed in Phire Tissue Direct Dilution Buffer
453 (ThermoFisher Scientific). Amplification of ORFs was done using Phire Tissue Direct PCR Master
454 Mix (ThermoFisher Scientific) and products were purified using QIAquick PCR Purification Kit
455 (Qiagen). Purified PCR products were subjected to Nextera XT library preparation and deep

456 sequencing using the Illumina HiSeq 2500 system (150 bp single read). Sequencing data was
457 processed and hits were identified using custom software developed using R programming
458 language and integrated Bowtie2 alignment tool, version 2.5.2.[52]
459
460 **Counter-screen assay**
461 BTSCs were transfected with siRNA using RNAiMax in a 96-well plate. Briefly, 1 pmol
462 of siRNA and 0.1 µl of RNAiMax were diluted in 5 µl of Opti-MEM and incubated separately for
463 5 minutes. The solutions were then gently combined and incubated at room temperature for 15
464 minutes to form transfection complexes. A total of 1,000 BTSCs per well were seeded in 80 µl of
465 NeuroCult medium, followed by the addition of 10 µl of the siRNA-RNAiMax complex with
466 gentle shaking. After incubation at 37°C for 5 hours, 90 µl of NeuroCult medium was added to
467 each well, and cells were further incubated at 37°C for 48 hours. Transfected cells were then
468 subjected to the PrestoBlue assay to assess cell viability.
469
470 **Duolink Proximity Ligation Assay (PLA)**
471 Proximity Ligation Assay was conducted following the manufacturer's protocol using the
472 Duolink *In Situ* Red Starter Kit (Sigma, #DUO92101) as optimized by our group[53], and described
473 in the Supplemental Materials and methods section.
474
475 **Extreme Limiting Dilution Assay (ELDA)**
476 ELDA was performed as previously described[54], with detailed methods presented in the
477 Supplemental Materials and methods section.
478

479 **5-ethynyl-2'-deoxyuridine (EdU) Assay**

480 Cell proliferation of BTSC73, BTSC147, and their related CLIC1 CRISPR KD cell were
481 assessed using the Click-iT™ Plus EdU Alexa Fluor™ 488 Flow Cytometry Assay Kit (Invitrogen,
482 Cat #C10632). According to the manufacturer's protocol, cells were incubated with 10μM EdU for
483 2 hours at 37 °C to label newly synthesized DNA. Following this step, cells were fixed,
484 permeabilized, and washed twice with a permeabilization and wash buffer provided in the kit. The
485 incorporated EdU was then detected with the Alexa Fluor 488 azide via a copper-catalyzed click
486 reaction. Following a final two washes, samples were analyzed using Cytek Aurora Flow
487 Cytometry System (5) Lasers/ (64) Fluorescence Channels/ (67) Detector (Cytek Biosciences#
488 62352, USA). Data were analyzed using FlowJo™ v10 Software.

489

490 **In vitro binding assay**

491 HEK293T cells were seeded in 6-well plates at approximately 60–70% confluency one day
492 prior to transfection. Cells were transfected using PEI with plasmids encoding Myc-tagged
493 truncated CLIC1 constructs, CLIC1(1–58) and CLIC1(1–178), together with expression vectors
494 for OSMR and/or EGFRvIII. The total amount of DNA per well was normalized with empty vector
495 to ensure equal transfection conditions across samples. Twenty-four hours post-transfection, cells
496 were washed twice with ice-cold phosphate-buffered saline (PBS) and lysed on ice in lysis buffer
497 (20 mM Tris-HCl, pH 7.5, 150 mM NaCl, 0.5% NP-40, 1 mM EDTA) supplemented with protease
498 and phosphatase inhibitor cocktails. Lysates were incubated on ice for 20 minutes and clarified by
499 centrifugation at 12,000 × g for 15 minutes at 4°C. The supernatants were collected for
500 immunoprecipitation (IP). 500 μg of total cell lysate was incubated with 1 μg of anti-Myc antibody
501 overnight at 4°C with gentle rotation to IP Myc-tagged CLIC1 and associated proteins. The

502 following day, Protein G Dynbeads were added and incubated for an additional 2 hours at 4°C.
503 Beads were then washed three times with lysis buffer. IPed proteins were eluted by boiling the
504 beads in 2x SDS sample buffer for 5 minutes and subjected to SDS–PAGE, followed by Western
505 blotting (WB). Proteins were transferred to PVDF membranes, which were blocked in 5% BSA in
506 TBST (20 mM Tris-HCl, 150 mM NaCl, 0.1% Tween-20, pH 7.4) for 1 hour at room temperature.
507 Membranes were then incubated overnight at 4°C with primary antibodies against Myc (for
508 CLIC1), OSMR, and EGFRvIII, followed by HRP-conjugated secondary antibodies for 2 hours at
509 room temperature, and were visualized using ECL. A fraction of total lysate (5% of total protein
510 used for IP) was analyzed in parallel to confirm expression of transfected constructs (input
511 control).
512
513 **Stereotaxic injections and bioluminescent imaging**
514 Stereotaxic surgeries were conducted by injecting ~3 x 10^5 luciferase expressing CLIC1
515 CRISPR BTSCs and control BTSCs into the right striata (0.8 mm lateral to the bregma, 1 mm
516 dorsal, and 2.5 mm from the pial surface). Prior to injection, BTSCs were dissociated into single-
517 cell suspensions in serum-free, antibiotic-free medium and tested for luciferase activity using IVIS
518 imaging system. Kaplan-Meier survival plots were generated by collecting mice at the point of
519 reaching the end stage (major body weight loss, dehydration, hunched back, piloerection, and
520 lethargy). Median survivals were calculated using a log-rank test with GraphPad Prism, following
521 previously described methods.[55] Briefly, the Kaplan-Meier approach estimated the probability of
522 survival at each time point. Before any time elapses, all mice were considered "at risk", however,
523 no deaths occurred. Therefore, the probability of survival was input as a value of 1. Subsequently,
524 information about the next elapsed time (day 7) included information about the how many

525 participants experienced the event of interest (death). From this information, a survival probability
526 was calculated using the formula: $S_{t+1} = S_t*((N_{t+1}-D_{t+1})/N_{t+1})$, where S_t represents survival
527 probability, N_t represents number at risk, D_t represents number of events. The survival probability
528 for each subsequent time point is calculated, and a stair-step survival curve is plotted. For tumour
529 volume assessment, the mice received intraperitoneal injections of 200 µl of 15 mg/ml d-luciferin
530 (ThermoFisher Scientific, #88292), underwent anesthesia via isoflurane inhalation, and were then
531 subjected to weekly bioluminescence imaging using a CCD camera (IVIS, Xenogen). Subsequent
532 collection and analysis of all bioluminescent data were performed utilizing Living Image 2.0
533 software (PerkinElmer, MA, USA). Briefly, after initialization of the IVIS Spectrum system and
534 acquiring an image, the images were analyzed using "ROI tools" in the tool palette, selecting the
535 area of interest. The IVIS imager captures pixels with specific photon intensity values, with
536 brighter areas corresponding to higher photon detection, indicative of tumour induction.

537 **Design and generation of the tmCLIC1 monoclonal antibody**

538 We designed and generated tmCLIC1 mAb to specifically target the NH_2-terminal region
539 of the CLIC1 protein. Polyclonal antibodies were initially generated through a 138-day
540 immunization protocol in which mice were immunized with a synthetic peptide corresponding to
541 the NH_2-terminus of CLIC1 (NH_2-EQPQVELFVKAGSDGAKIGNC-COOH), conjugated to
542 ovalbumin (OVA) and dissolved in a buffer composed of 0.1 M glycine (pH 3) and 1 M Tris-HCl
543 (pH 8). Antibody specificity was confirmed by the supplier using an ELISA assay. Hybridoma
544 cells producing antibodies were sorted as single cells to isolate monoclonal clones. A total of 44
545 distinct monoclonal antibodies, derived from all four immunized mice, were sent to our laboratory
546 for further screening. Among these, we selected the clone showing the highest specificity and
547 sensitivity. Sequencing of the selected clone revealed strong binding affinity to the QVELF motif

548 of the immunizing peptide, a sequence conserved across several species and uniquely expressed
549 by tmCLIC1, but not by other members of the CLIC protein family. Multiple experiments were
550 conducted to assess the specificity and functional effectiveness of tmCLIC1omab in inhibiting
551 tmCLIC1 activity (**Fig. 6l-n, supp. Fig. 9a,b**). We also demonstrated that the antibody retains its
552 effect on primary human glioblastoma cells even after short incubation periods (**Fig. 6o**), and that
553 it is efficiently internalized into cells, as shown using the pHrodo™ dye assay (**supp. Fig. 9c,d**).
554 Additionally, we evaluated the *in vivo* tolerability of tmCLIC1omab in a mouse model of human
555 colorectal cancer. Mice received biweekly injections of the antibody for three weeks. Body weight
556 monitoring showed no significant difference between tmCLIC1omab-treated mice and those
557 receiving an isotype control, indicating that the antibody is well tolerated *in vivo* (**Fig. 6p**) (The
558 expanded version can be found in the Supplemental Materials and methods section).
559

560 **Patch-Clamp Experiment**

561 Patch electrodes (BB150F-8P with filaments, Science Products), with a diameter of 1.5
562 mm, were pulled from hard borosilicate glass on a Brown-Flaming P-87 puller (Sutter Instrument,
563 Novato, CA) and fire polished to a tip diameter of 1-1.5 μm and an electrical resistance of 3-4 MΩ.
564 Cells were voltage-clamped using an Axopatch 200B amplifier (Axon Intrument) in whole-cell
565 configuration in which After formation of giga-seal, the membrane patch is disrupted providing a
566 direct low resistance access to cell interior, allowing recordings from ion channels of whole cell.
567 The voltage step protocol used to isolate current/voltage relationships consisted of 800 ms pulses
568 from -60 mV to +60 mV (20 mV voltage steps). The holding potential was set according to the
569 resting potential of the single cell (between -40 and -80 mV). tmCLIC1-mediated chloride currents
570 were isolated from other ionic currents by perfusing IAA94 (100 μM) dissolved in the bath solution

571 and by mathematical subtraction of the residual current from the control. Solution used are the
572 following: bath solution (mM): 125 NaCl, 5.5 KCl, 24 HEPES, 1 MgCl2, 0.5 CaCl2, 5 D-Glucose,
573 10 NaOH; pH 7.4; Pipette solution (mM): 135 KCl, 10 Hepes, 10 NaCl; pH 7.4. Analysis was
574 performed using Clampfit 10.2 (Molecular Devices) and OriginPro 9.1. tmCLIC1-mediated
575 current (IAA94-sensitive current) was measured by analytical subtraction of residual ionic current
576 after addition of inhibitor from total current (I_{TOT}) of the cell at each membrane potential tested.
577 Current/voltage relationship were constructed plotting the averaged current density of the least 100
578 ms of the pulse against the corresponding membrane potential. Current density (pA/pF) results
579 from the ratio between the ionic current (pA) and cells capacitance (pF). Statistical analyses were
580 performed comparing the slopes (proportional to channel conductance) of the I/V curves of the
581 different groups.
582
583 **Generation of monoclonal tmCLIC1 antibody**
584 The tmCLIC1omab® antibody was designed (license# 11665M), targeting the N-terminal
585 of the CLIC1 protein derived from mice. Polyclonal antibodies were obtained through a 138-day
586 immunization protocol in which mice are immunized against a NH_2-CLIC1 synthetic peptide
587 conjugated to OVA (ovalbumin) (NH_2-EQPQVELFVKAGSDGAKIGNC-COOH) (Glycine 0.1
588 M pH 3, Tris-HCl 1 M pH 8). Hybridoma cells that produced antibodies were sorted in single cells
589 to obtain monoclonal antibodies. tmCLIC1omab® was used at a final concentration of 3.5 µg/ml.
590
591 **Extracellular vesicle isolation and validation**
592 To sequentially isolate EVs, the cell supernatant was centrifuged at 200 x g for 10 minutes,
593 300 x g for 10 minutes, 2,000 x g for 10 minutes, 10,000 x g for 30 minutes, and 100,000 x g for

594 2 hours, respectively (Optima XPN-100 ultracentrifuge, Beckman Coulter, USA). A beige/white
595 pellet of EVs and a clear supernatant were evident post-centrifugation. After removing the
596 supernatant and resuspending the small EV pellet in 1 ml PBS, the resulting pellet was then washed
597 and centrifuged at 49,000 rpm for 30 minutes (Optima MAX 130K Refrigerated Benchtop
598 Ultracentrifuge, Beckman Coulter, USA). Isolated EVs were then visualized, measured, counted,
599 and characterized in the range of 10-2,000 nm using a Nanoparticle Tracking Analyzer (NTA)
600 (Particle Metrix ZetaView® Nanoparticle Tracking Analysis).[56,57] We used size-mode analysis
601 with ZetaView software (version 8.02.28) following calibration with polystyrene beads (105 and
602 500 nm). Samples were analyzed at a minimum of 9 camera positions with 2-second video length
603 at 21°C.
604
605 **Bioinformatic analysis**
606 Novel interactions from MAMTH screen were integrated with the known interactions from
607 the Integrated Interaction Database IID ver. 2021-05[58] and further annotated with Gene Ontology
608 Biological Process and Cellular Component (release 2022-11-03), and a subset of pathways from
609 the PathDIP database ver. 4.[59] Resulting network was built, annotated and analyzed using
610 NAViGaTOR ver. 3.0.19.[60]
611
612 **Statistical analysis**
613 Statistical analysis between conditions was performed using a Student *t*-test or one-way
614 ANOVA in which the mean of n=3 replicates were compared between two conditions to assess
615 significance. Analysis was undertaken with the aid of GraphPad software 7. Data is shown as mean
616 with standard deviation (mean ± SD). p-values less than 0.05 were considered significant and were

617 marked with an asterisk as follows, *$P < 0.05$; **$P < 0.01$; ***$P < 0.001$. Precise p values are

618 provided in the figure legends, unless noted otherwise.

619

620 **REFERENCES**

621

622 1 Hara, T. *et al.* Interactions between cancer cells and immune cells drive transitions to
623 mesenchymal-like states in glioblastoma. *Cancer cell* **39**, 779-792. e711 (2021).
624 2 Araujo, A. M. *et al.* Stromal oncostatin M cytokine promotes breast cancer progression by
625 reprogramming the tumor microenvironment. *The Journal of clinical investigation* **132**
626 (2022).
627 3 Alonso-Nocelo, M. *et al.* Macrophages direct cancer cells through a LOXL2-mediated
628 metastatic cascade in pancreatic ductal adenocarcinoma. *Gut* **72**, 345-359 (2023).
629 4 Jahani-Asl, A. *et al.* Control of glioblastoma tumorigenesis by feed-forward cytokine
630 signaling. *Nature neuroscience* **19**, 798-806 (2016).
631 5 Sharanek, A. *et al.* OSMR controls glioma stem cell respiration and confers resistance of
632 glioblastoma to ionizing radiation. *Nature communications* **11**, 4116 (2020).
633 6 Carro, M. S. *et al.* The transcriptional network for mesenchymal transformation of brain
634 tumours. *Nature* **463**, 318-325, doi:10.1038/nature08712 (2010).
635 7 Sherry, M. M., Reeves, A., Wu, J. K. & Cochran, B. H. STAT3 is required for proliferation
636 and maintenance of multipotency in glioblastoma stem cells. *Stem Cells* **27**, 2383-2392,
637 doi:10.1002/stem.185 (2009).
638 8 de la Iglesia, N., Puram, S. V. & Bonni, A. STAT3 regulation of glioblastoma pathogenesis.
639 *Curr Mol Med* **9**, 580-590 (2009).
640 9 Hara, T. *et al.* Interactions between cancer cells and immune cells drive transitions to
641 mesenchymal-like states in glioblastoma. *Cancer Cell* **39**, 779-792 e711,
642 doi:10.1016/j.ccell.2021.05.002 (2021).
643 10 Lee, B. Y. *et al.* Heterocellular OSM-OSMR signalling reprograms fibroblasts to promote
644 pancreatic cancer growth and metastasis. *Nature communications* **12**, 7336 (2021).
645 11 Dey, G. *et al.* Signaling network of Oncostatin M pathway. *Journal of Cell Communication*
646 *and Signaling* **7**, 103-108 (2013).
647 12 Hermanns, H. M. Oncostatin M and interleukin-31: Cytokines, receptors, signal
648 transduction and physiology. *Cytokine & growth factor reviews* **26**, 545-558 (2015).
649 13 Natesh, K. *et al.* Oncostatin-M differentially regulates mesenchymal and proneural
650 signature genes in gliomas via STAT3 signaling. *Neoplasia* **17**, 225-237 (2015).
651 14 Chen, M. *et al.* Exploring the oncostatin M (OSM) feed-forward signaling of glioblastoma
652 via STAT3 in pan-cancer analysis. *Cancer cell international* **21**, 1-19 (2021).
653 15 Yang, X. *et al.* A public genome-scale lentiviral expression library of human ORFs. *Nature*
654 *methods* **8**, 659-661 (2011).
655 16 Lim, S. H. *et al.* CFTR interactome mapping using the mammalian membrane two-hybrid
656 high-throughput screening system. *Molecular systems biology* **18**, e10629 (2022).

657 17 Setti, M. *et al.* Functional role of CLIC1 ion channel in glioblastoma-derived
658 stem/progenitor cells. *Journal of the National Cancer Institute* **105**, 1644-1655 (2013).
659 18 Littler, D. R. *et al.* The intracellular chloride ion channel protein CLIC1 undergoes a redox-
660 controlled structural transition. *Journal of Biological Chemistry* **279**, 9298-9305 (2004).
661 19 Ashley, R. Challenging accepted ion channel biology: p64 and the CLIC family of putative
662 intracellular anion channel proteins. *Molecular membrane biology* **20**, 1-11 (2003).
663 20 Gururaja Rao, S., Patel, N. J. & Singh, H. Intracellular chloride channels: novel biomarkers
664 in diseases. *Frontiers in physiology* **11**, 96 (2020).
665 21 Randhawa, K. & Jahani-Asl, A. CLIC1 regulation of cancer stem cells in glioblastoma.
666 *Current Topics in Membranes* **92**, 99-123 (2023).
667 22 Hu, Y. & Smyth, G. K. ELDA: extreme limiting dilution analysis for comparing depleted
668 and enriched populations in stem cell and other assays. *Journal of immunological methods*
669 **347**, 70-78 (2009).
670 23 Setti, M. *et al.* Extracellular vesicle-mediated transfer of CLIC1 protein is a novel
671 mechanism for the regulation of glioblastoma growth. *Oncotarget* **6**, 31413 (2015).
672 24 Zhao, K. *et al.* Exosome-mediated transfer of CLIC1 contributes to the vincristine-
673 resistance in gastric cancer. *Molecular and cellular biochemistry* **462**, 97-105 (2019).
674 25 Kang, M.-K. & Kang, S.-K. Pharmacologic blockade of chloride channel synergistically
675 enhances apoptosis of chemotherapeutic drug-resistant cancer stem cells. *Biochemical and*
676 *biophysical research communications* **373**, 539-544 (2008).
677 26 Al-Nedawi, K. *et al.* Intercellular transfer of the oncogenic receptor EGFRvIII by
678 microvesicles derived from tumour cells. *Nature cell biology* **10**, 619-624 (2008).
679 27 Wang, W. *et al.* The expression and clinical significance of CLIC1 and HSP27 in lung
680 adenocarcinoma. *Tumor Biology* **32**, 1199-1208 (2011).
681 28 Jia, N. *et al.* CLIC1 overexpression is associated with poor prognosis in pancreatic ductal
682 adenocarcinomas. *Journal of cancer research and therapeutics* **12**, 892-896 (2016).
683 29 Singha, B. *et al.* CLIC1 and CLIC4 complement CA125 as a diagnostic biomarker panel
684 for all subtypes of epithelial ovarian cancer. *Scientific reports* **8**, 14725 (2018).
685 30 Francisco, M. A. *et al.* Chloride intracellular channel 1 cooperates with potassium channel
686 EAG2 to promote medulloblastoma growth. *Journal of Experimental Medicine* **217** (2020).
687 31 Wang, L. *et al.* Elevated expression of chloride intracellular channel 1 is correlated with
688 poor prognosis in human gliomas. *Journal of Experimental & Clinical Cancer Research*
689 **31**, 1-7 (2012).
690 32 Boucrot, E. & Kirchhausen, T. Mammalian cells change volume during mitosis. *PloS one*
691 **3**, e1477 (2008).
692 33 Habela, C. W. & Sontheimer, H. Cytoplasmic volume condensation is an integral part of
693 mitosis. *Cell cycle* **6**, 1613-1620 (2007).
694 34 Milton, R. H. *et al.* CLIC1 function is required for β-amyloid-induced generation of
695 reactive oxygen species by microglia. *Journal of Neuroscience* **28**, 11488-11499 (2008).
696 35 Novarino, G. *et al.* Involvement of the intracellular ion channel CLIC1 in microglia-
697 mediated β-amyloid-induced neurotoxicity. *Journal of Neuroscience* **24**, 5322-5330
698 (2004).
699 36 Valenzuela, S. M. *et al.* The nuclear chloride ion channel NCC27 is involved in regulation
700 of the cell cycle. *The Journal of physiology* **529**, 541 (2000).

701 37 Peretti, M. *et al.* Mutual Influence of ROS, pH, and CLIC1 Membrane Protein in the
702 Regulation of G1–S Phase Progression in Human Glioblastoma Stem Cells. *Molecular*
703 *cancer therapeutics* **17**, 2451-2461 (2018).
704 38 Singh, H. & Ashley, R. H. Redox regulation of CLIC1 by cysteine residues associated with
705 the putative channel pore. *Biophysical journal* **90**, 1628-1638 (2006).
706 39 Jiang, L. *et al.* Intracellular chloride channel protein CLIC1 regulates macrophage function
707 through modulation of phagosomal acidification. *Journal of cell science* **125**, 5479-5488
708 (2012).
709 40 Westman, J. & Grinstein, S. Determinants of phagosomal pH during host-pathogen
710 interactions. *Frontiers in cell and developmental biology* **8**, 624958 (2021).
711 41 Salao, K. *et al.* CLIC1 regulates dendritic cell antigen processing and presentation by
712 modulating phagosome acidification and proteolysis. *Biology open* **5**, 620-630 (2016).
713 42 Domingo-Fernández, R., Coll, R. C., Kearney, J., Breit, S. & O'Neill, L. A. The
714 intracellular chloride channel proteins CLIC1 and CLIC4 induce IL-1β transcription and
715 activate the NLRP3 inflammasome. *Journal of Biological Chemistry* **292**, 12077-12087
716 (2017).
717 43 Kelley, N., Jeltema, D., Duan, Y. & He, Y. The NLRP3 inflammasome: an overview of
718 mechanisms of activation and regulation. *International journal of molecular sciences* **20**,
719 3328 (2019).
720 44 Hamarsheh, S. a. & Zeiser, R. NLRP3 inflammasome activation in cancer: a double-edged
721 sword. *Frontiers in immunology* **11**, 1444 (2020).
722 45 Stockhausen, M.-T., Kristoffersen, K., Stobbe, L. & Poulsen, H. S. Differentiation of
723 glioblastoma multiforme stem-like cells leads to downregulation of EGFR and EGFRvIII
724 and decreased tumorigenic and stem-like cell potential. *Cancer biology & therapy* **15**, 216-
725 224 (2014).
726 46 Gritti, M. *et al.* Metformin repositioning as antitumoral agent: selective antiproliferative
727 effects in human glioblastoma stem cells, via inhibition of CLIC1-mediated ion current.
728 *Oncotarget* **5**, 11252 (2014).
729 47 He, M. *et al.* Chloride channels regulate differentiation and barrier functions of the
730 mammalian airway. *Elife* **9**, e53085 (2020).
731 48 Barbieri, F. *et al.* Repurposed biguanide drugs in glioblastoma exert antiproliferative
732 effects via the inhibition of intracellular chloride channel 1 activity. *Frontiers in oncology*
733 **9**, 135 (2019).
734 49 Sharanek, A. *et al.* Transcriptional control of brain tumor stem cells by a carbohydrate
735 binding protein. *Cell reports* **36** (2021).
736 50 Engler, C., Gruetzner, R., Kandzia, R. & Marillonnet, S. Golden gate shuffling: a one-pot
737 DNA shuffling method based on type IIs restriction enzymes. *PloS one* **4**, e5553 (2009).
738 51 Petschnigg, J. *et al.* The mammalian-membrane two-hybrid assay (MaMTH) for probing
739 membrane-protein interactions in human cells. *Nature methods* **11**, 585-592 (2014).
740 52 Langmead, B. & Salzberg, S. L. Fast gapped-read alignment with Bowtie 2. *Nature*
741 *methods* **9**, 357-359 (2012).
742 53 Sharanek, A., Raco, L., Soleimani, V. D. & Jahani-Asl, A. In situ detection of protein-
743 protein interaction by proximity ligation assay in patient derived brain tumor stem cells.
744 *STAR protocols* **3**, 101554 (2022).
745 54 Rasool, D., Soleimani, V. D. & Jahani-Asl, A. in *Neuronal Cell Death: Methods and*
746 *Protocols* 343-354 (Springer, 2022).

55 Luchman, H. A. *et al.* An in vivo patient-derived model of endogenous IDH1-mutant glioma. *Neuro-oncology* **14**, 184-191 (2011).
56 Myette, R. L. *et al.* Urinary podocyte-derived large extracellular vesicles are increased in paediatric idiopathic nephrotic syndrome. *Nephrology Dialysis Transplantation* **38**, 2089-2091 (2023).
57 Ruzicka, M. *et al.* Effect of hemodialysis on extracellular vesicles and circulating submicron particles. *BMC nephrology* **20**, 1-8 (2019).
58 Kotlyar, M. *et al.* IID 2021: towards context-specific protein interaction analyses by increased coverage, enhanced annotation and enrichment analysis. *Nucleic acids research* **50**, D640-D647 (2022).
59 Rahmati, S. *et al.* pathDIP 4: an extended pathway annotations and enrichment analysis resource for human, model organisms and domesticated species. *Nucleic acids research* **48**, D479-D488 (2020).
60 Brown, K. R. *et al.* NAViGaTOR: network analysis, visualization and graphing Toronto. *Bioinformatics* **25**, 3327-3329 (2009).

Acknowledgements

This work was supported by Canadian Institute for Health Research (CIHR) grants (# 157480, #157797), Canada Foundation for Innovation (CFI) (#156794), Ontario Research Fund (ORF) (#156796), Canada Research chair (CRC) (#156787, 156789), to A.J.-A, and CIHR grants to AJA, I.S., J.R. (# 162198, #519474) and a AIRC IG grant (#24758) to M.M.. A.J.-A. is a Canada Research Chair at the University of Ottawa and is supported by CIHR, Natural Sciences Research Council (NSERC), Cancer Research Society (CRS). I.S. is supported by CFI (#225404, #30865), ORF (RDI #34876, RE010-020), and (NSERC RGPIN-2024-04314). IJ was supported in part by funding from NSERC (RGPIN-2024-04314), CIHR (#519474), CFI #225404, #30865, and ORF (RDI #34876, RE010-020). HS is supported by NCATS (R03TR005313), NHLBI (R01HL133050). The funders had no role in study design, data collection and analysis, decision to publish, or preparation of the manuscript.

801 **Figure legends**

802 **Figure 1. Mapping global binding partners of OSMR.**

803 Using MaMTH-HTS, we mapped the OSMR interactome in the absence and presence of
804 EGFRvIII. The interactome is represented with green edges for the novel MaMTH candidates and
805 gray edges highlighting known interactions identified using the Integrated Interaction Database
806 (IID). Purple edges indicate interactions both identified in MaMTH and predicted by IID. The
807 candidate binding partners of OSMR in the absence of EGFRvIII (OSMR-specific interactors) are
808 represented in blue. The candidate binding partners of OSMR in the presence of EGFRvIII
809 (OSMR/EGFRvIII-specific interactors) are represented in red. The candidate binding partners of
810 OSMR that were commonly shared by both groups are shown in the center. Go term functional
811 annotation of the potential candidates are shown with different coloured squares.

812

813 **Figure 2. CLIC1 and OSMR are upregulated in glioblastoma, and their high expression**
814 **correlates with poor patient survival.**

815 **a,b**, Expression of CLIC1 and OSMR in GB and non-tumour samples from four glioblastoma
816 datasets (Gravendeel, Kamoun, Rembrandt, TCGA) was compared. Both genes were significantly
817 elevated in GB samples, except for OSMR in the Kamoun dataset. **c,d**, Expression of CLIC1 and
818 OSMR across different glioblastoma subtypes of Proneural, Classical, and Mesenchymal were
819 ordered by disease severity in four datasets. CLIC1 displays consistent, significant upregulation
820 with subtype progression, while OSMR is significantly upregulated in both Classical and
821 Mesenchymal subtypes relative to proneural subtype. **e-h**, Clinical significance of variable CLIC1
822 expression in high- and low-OSMR expressing patients were analyzed using annotated public
823 online datasets is shown.

824 **Figure 3. Cell viability evaluation following gene silencing of candidate binding protein**
825 **targets.**
826 **a-d**, Knockdown of CLIC1 was induced in BTSCs as described, and whole cell lysates were
827 subjected to immunoblotting using a CLIC1 antibody. ACTIN was used as a loading control. **e-h**,
828 CLIC1 knockdown and control cells were subjected to Extreme Limiting Dilution Assay, n=3
829 biological replicates. Statistical analysis was performed using a student-t test. Data are represented
830 as the means ± SD. BTSC73 (**e**): ***P = 0.0010; BTSC147 (**f**): **P = 0.0017; BTSC12 (**g**): **P
831 = 0.0077; BTSC30 (**h**): ***P = 0.0006 for each pairwise comparison. **i-j,** Validation of CRISPR-
832 mediated CLIC1 KD and KO in patient-derived BTSC73 and BTSC147 cell lines. CLIC1 protein
833 expression levels were evaluated by immunoblotting following CLIC1 KD (CLIC1 CRISPR-m)
834 and CLIC1 KO (CLIC1 CRISPR-b), comparing them with the control group (CTL), with n=3
835 biological replicates. **k,l**, mRNA expression of CLIC1 was confirmed by RT-qPCR in CLIC1
836 CRISPR BTSCs 147 and 73. Gene expression was normalized to the housekeeping gene GUSB.
837 Data for two different clones (CRISPR-m and CRISPR-b) are shown for each BTSCs and
838 represented as the means ± SD, n = 3. Statistical analysis was performed using one-way ANOVA.
839 BTSC73 (**k**): ****P = 0.00003 and 0.00001, respectively, for each pairwise comparison from left
840 to right. BTSC147 (**l**): ****P = 0.000000006 and 0.000000005, respectively, from left to right;
841 **m,n**, CLIC1 CRISPR and control BTSCs were subjected to ELDA and SCF was plotted. n=3
842 biological replicates/ Statistical analysis was preformed using one-way ANOVA. Data are
843 represented as the means ± SD. BTSC73 CRISPR-m and CRISPR-b (**m**): **P = 0.0084, **P =
844 0.0011 for each pairwise comparison respectively. BTSC147 (**n**): ***P = 0.0002; **o,** Flow
845 cytometry analysis of DNA replication in EdU-labeled cells from BTSC73-CTL and BTSC73-

846 CRISPR-m is shown. n=3 biological replicates. **p,** Statistical analysis was performed using a
847 student-t test. Data are represented as the means ± SD, *P = 0.0107.
848
849 **Figure 4. CLIC1 and OSMR interact endogenously in BTSCs.**
850 **a-c**, Non-permeabilized BTSCs were subject to immunostaining and CLIC1 is detected at the
851 plasma membrane. Images in Merged shows representative CLIC1 expression (green) overlapping
852 with Hoechst (blue). Each experiment was conducted with a primary antibody omitted control
853 group, n=3 biological replicates. **d-g**, BTSCs were subjected to co-immunostaining using
854 antibodies to CLIC1 (green) and OSMR (red). Nuclei were stained with Hoechst. Merged images
855 depict co-localization of OSMR and CLIC1 (yellow). n=3 biological replicates. **h-l**, BTSCs were
856 subjected to proximity ligation assay (PLA) using antibodies to CLIC1 and OSMR. Each red
857 puncta represents PLA signal. Primary antibodies were omitted for control group. Nuclei were
858 stained with Hoechst. **m-p**, The interaction of CLIC1 and OSMR was assessed by PLA in CLIC1
859 CRISPR and control BTSCs as described in h-l. Nuclei were stained with Hoechst. The number of
860 PLA puncta (red) per nucleus was quantified in CRISPR and control BTSC73 and BTSC147 (**n,p**).
861 Data are presented as the means ± SEM. Each dot represents the number of PLA dots per nucleus.
862 A minimum of n=3 biological replicate images was assessed for statistical analysis. Statistical
863 analysis was performed using one-way ANOVA. BTSC73 (**n**): ****P =0.000002 and 0.0000009
864 respectively, for each pairwise comparison from left to right. Scale bar, 10 μm; BTSC147 (**p**):
865 ****P = 0.00000003 and 0.00000001 respectively, from left to right. **q,r**, BTSCs 73 or 147 were
866 subjected to immunoprecipitation (IP) using an OSMR antibody or IgG control and pull downs
867 were analyzed by immunoblotting using CLIC1 antibody. **s,t**, BTSCs 73 and 147 were subjected
868 to co-immunostaining using antibodies to CLIC1 and EGFRvIII. Representative images represent

869 n=3 independent biological replicates. **u,v**, CLIC1 CRISPR and control BTSCs were subjected to
870 PLA analysis using antibodies to CLIC1 and EGFRvIII.
871
872 **Figure 5. CLIC1 mediates the formation of the OSMR/EGFRvIII complex through its**
873 **extracellular domain.**
874 **a-e,** BTSCs 73, 147, and their related CLIC1 CRISPR cells were subjected to PLA analysis using
875 antibodies to OSMR and EGFRvIII (**a,b**) and quantification of # of PLA per nuclei are presented
876 (**c-e**). Nuclei were stained with Hoechst. Scale bar, 10 μm. Statistical analysis was performed using
877 one-way ANOVA. BTSC73 (**d**): ****P = 0.000000001 and 1 x 10^{-13} respectively, from left to
878 right; BTSC147 (**e**): ****P = 1 x 10^{-15} for each pairwise comparison. **f**, The interaction of the
879 CLIC1 dimer (purple and brown), OSMR (green), and EGFRvIII (orange) was predicted using
880 AlphaFold-Multimer for their extracellular domains. The predicted 3D structures of the
881 extracellular domains, including surface representations of the interaction regions and close-up
882 views of the binding interfaces between CLIC1 and EGFRvIII, and between EGFRvIII and OSMR,
883 are shown. **g,h,** Experimental validation of the predicted domain using co-IP was performed.
884 HEK293T cells were transfected with plasmids encoding CLIC1, OSMR, and/or EGFRvIII.
885 Protein extracts were subjected to CLIC1 IP, followed by WB detection of CLIC1, OSMR, and
886 EGFRvIII (**g**). HEK293T cells were transfected with plasmids encoding truncated CLIC1
887 constructs, CLIC1(1–58) and CLIC1(1–178), together with OSMR and/or EGFRvIII. Protein
888 extracts were subjected to CLIC1 IP, and CLIC1, OSMR, and EGFRvIII were detected by WB
889 (**h**). **i**, Native gel electrophoresis for CLIC1, OSMR, and EGFRvIII is shown.
890

891 **Figure 6. Blocking of tmCLIC1 using a monoclonal antibody reduces tumourigenesis,**
892 **decreases tumour size, and suppresses STAT3 phosphorylation.**
893 **a-c,** CLIC1 CRISPR and control BTSCs were subjected to extracellular vesicle (EV) isolation.
894 EV-digested lysates and whole cell lysates were subjected to immunoblotting analysis using
895 antibodies indicated on the blot (**a**). Quantification of EGFRvIII in EV were conducted (**b,c**).
896 Statistical analysis was performed using one-way ANOVA. n=3 biological replicates. BTSC147
897 (**b**): ***P = 0.00025, ****P = 0.000027; BTSC73 (**c**): ***P = 0.00098, ****P = 0.000059 for
898 each pairwise comparison. **d**, Electrophysiological evaluation of tmCLIC1 was conducted at +40
899 mV on CLIC1 CRIPSR and control BTSCs. WT (white bar), CLIC1 +/- (monoallelic deletion,
900 grey bar) and CLIC1 -/- (biallelic deletion, black bar). *P = 0.024, **P = 0.0091. **e-h**,
901 Representative whole cell current for cells were conducted at several voltages ranging from -60 to
902 +60 mV with 20 mV increments in control (**e,g**) and in OSMR knockdown BTSCs (**f,h**). Currents
903 were recorded in resting conditions (**e,f**) and after IAA94 administration (**g,h**). **i**, I/V plot for
904 control (SCR, black circles) and after perfusion of IAA94 (empty circles), and **j**, I/V plot for
905 shOSMR cells in CTL condition (black triangles) and after perfusion of IAA94 (empty triangles)
906 are shown. Average current-voltage recordings at different test potentials are shown. **k**, tmCLIC1
907 current for four different GB cell lines were analyzed at +40 mV in shOSMR and SCR control
908 groups. The average current for the SCR (grey) and shOSMR (black) cells are shown. BTSC73 *P
909 = 0.0179; BTSC30 *P = 0.0173, L1312 *P = 0.0205. **l,m**, Growth curves of human primary GB
910 cell lines, WT and CLIC1 knockout, are shown. (**l**) GB human primary cell line WT growth curves
911 over 96 hours in the absence (black circles) or presence (red circles) of tmCLIC1omab and IAA94
912 (blue circles); CTL, 24-96 hours, n=4; tmCLIC1omab and IAA94, 24-96 hours, n=7. 72-96 hours,
913 ****p<0.0001. Means ± SEM, two-way ANOVA, Tukey's multiple comparison test. (**m**) GB

914 human primary cell line knockout for CLIC1 protein growth curves over 96 hours in the absence
915 (black circles) or presence (red circles) of tmCLIC1omab and IAA94 (blue circles). CTL, 24-96
916 hours, n=5; tmCLIC1omab and IAA94, 24-96 hours, n=6. Means ± SEM. **n**, Dose-response curve
917 of human primary GB cell line treated with increasing concentrations of tmCLIC1omab is shown.
918 Cell viability was measured after 72 hours of treatment. The response was fitted using a non-linear
919 regression model (four-parameter logistic model), and IC_{50} (half-maximal inhibitory
920 concentration) was calculated. Error bars represent the standard deviation (SD) of 4 biological
921 replicates. IC50=0.184 µM. **o**, tmCLIC1omab effect on proliferation after several time of
922 incubation is shown. Cell number of human primary GB cells incubated for 3, 5, 24 or 72 hours
923 with tmCLIC1omab. The antibody was washout after selected time of incubation and then the
924 number of cells was evaluated after 72 hours. One-way ANOVA; CTL (n=3) vs 3h (n=6)
925 ****p<0,0001; CTL vs 5h (n=3) *** p=0,0002; CTL vs 24 h (n=6) **** p<0,0001; CTL vs 72h
926 (n=3) *** p=0,0003. Tukey's multiple comparison test. **p**, Weight of the animals treated or not
927 treated with tmCLIC1omAb is shown. Body weight was measured prior to each injection and is
928 presented as mean ± SEM (n = 8 mice per group). No significant weight loss was observed over
929 the treatment period, indicating that tmCLIC1omab was well tolerated. Statistical significance was
930 assessed using two-way ANOVA, Sidak's multiple comparison test. **q-s,** BTSC73 cells were
931 xenografted subcutaneously into 8-week-old SCID male mice, and treatment with 200 µg
932 tmCLIC1omAb per animal, three times a week, was started on day 7 post-tumour inoculation.
933 IVIS imaging was conducted to evaluate tumour volume (**q**), with the signal quantified (**r**). The
934 tumours were then resected from the animals, and tumour size was measured using a standard
935 method (**s**). **t-y**, CLIC1 CRISPR and control BTSCs were treated with tmCLIC1omab for 72 hours
936 and were analyzed by immunoblotting using antibodies to p-STAT3, STAT3, p-EGFR and EGFR.

937 Densitometric analysis of p-STAT3 to total STAT3 (**t,v,w**) and p-EGFR to total EGFR (**u,x,y**) in
938 tmCLIC1mab treated antibodies versus control are shown. Statistical analysis was performed using
939 unpaired students' t test. n = 3 or > 3 biological replicates. BTSC73 (**t**): $^{**}P = 0.0022$; BTSC73
940 (**u**): $^{*}P = 0.0335$; BTSC147 (**w**): $^{**}P = 0.0038$.
941
942 **Figure 7. Genetic deletion of CLIC1 impairs tumourigenesis, expands lifespan and**
943 **suppresses EGFR/EGFRvIII activation.**
944 **a-h,** CLIC1 CRISPR BTSCs (#73,) control BTSC73, CLIC1 CRISPR BTSCs (#147), and control
945 BTSC147 were xenografted intracranially into 8 weeks old SCID male mice. IVIS imaging was
946 conducted to evaluate tumour volume (**a,d**) and signal was quantified (**b,e**). Kaplan-Meier survival
947 plots were graphed to evaluate animal lifespan in each group (**c,f**). Log-rank test (BTSC73) ($P <$
948 0.0001, $n \geq 5$ mice), BTSC#73 vs. CLIC1 CRISPR-a ($P = 0.0011$), BTSC#73 vs. CLIC1 CRISPR-
949 b ($P = 0.001$), CLIC1 CRISPR-a vs. CLIC1 CRISPR-b ($P = 0.0014$). Log rank test for BTSC#147,
950 ($P = 0.0078$, n=3), BTSC#147 vs. CLIC1 CRISPR-a ($P = 0.0246$), BTSC#147 vs CLIC1 CRISPR-
951 b ($P = 0.0246$), CLIC1 CRISPR-a vs CLIC1 CRISPR-b (non-significant). Representative panels
952 for changes in body weight following BTSC implantation are shown (**g-h**). **i-k**, Brain sections
953 depicting tumour in control BTSC73 and CLIC1 CRISPR BTSC73 were subjected to H&E
954 staining (**i,j**) or immunostaining with a p-EGFR-Y1068 antibody (**k**). **l-s**, CLIC1 CRISPR and
955 control BTSCs were subjected to immunoblotting using antibodies to P-STAT3-Y705, total
956 STAT3, EGFRvIII, and total EGFR. ACTIN was used as loading control. Densitometric
957 quantification of p-STAT3 to total STAT3 (**m,o**) and EGFRvIII to total EGFR (**q,s**) are presented.
958 Statistical analysis was performed using a student t-test. n=3 biological replicates. BTSC73 (**m**):

959 *P = 0.0121; BTSC147 (**o**): *P = 0.0423; BTSC73 (**q**): ***P = 0.0003; BTSC147 (**s**): ***P =

960 0.0001 for each pairwise comparison.

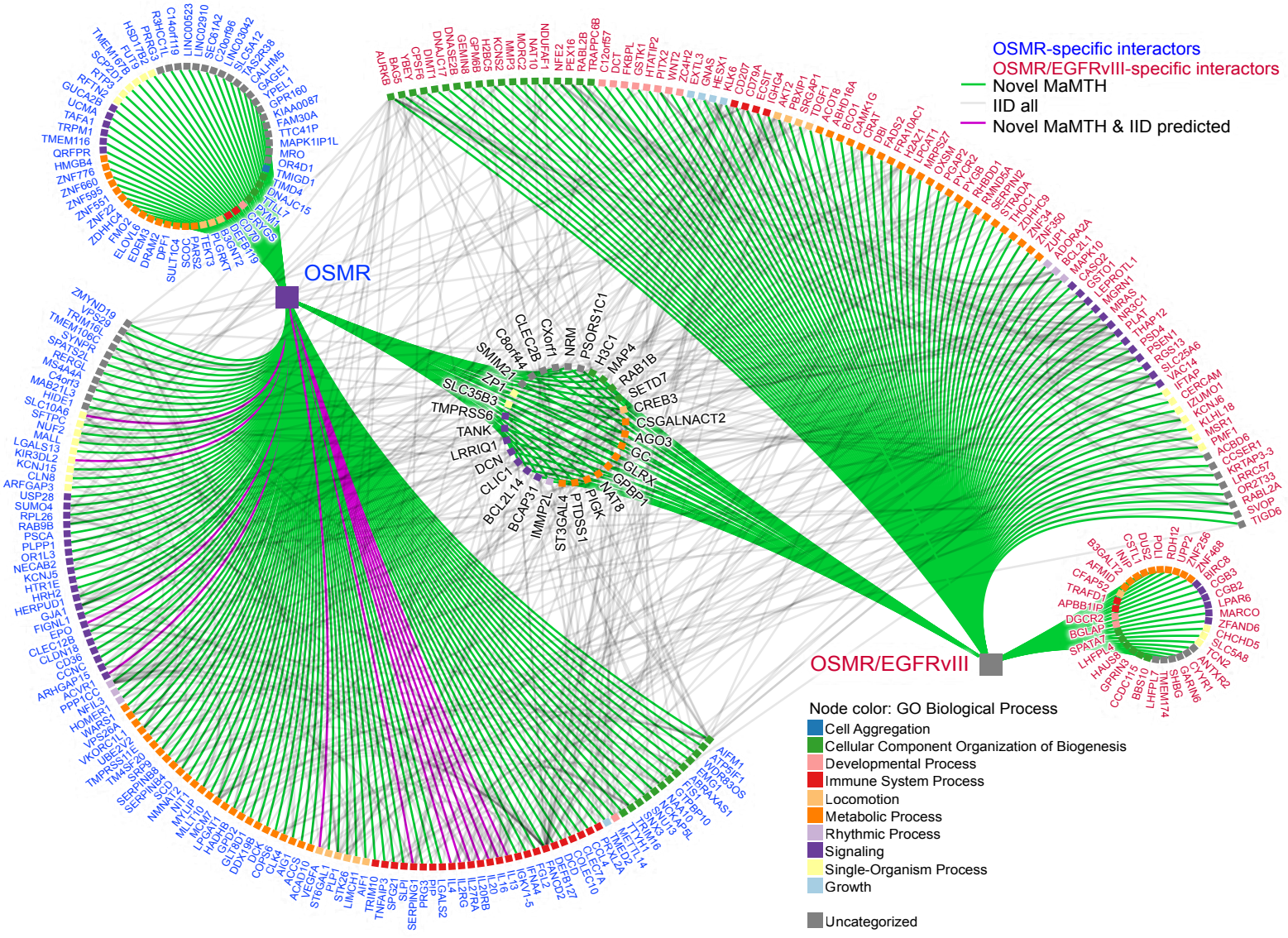
OSMR-specific interactors
OSMR/EGFRvIII-specific interactors
Novel MaMTH
IID all
Novel MaMTH & IID predicted
OSMR
OSMR/EGFRvIII
Node color: GO Biological Process
Cell Aggregation
Cellular Component Organization of Biogenesis
Developmental Process
Immune System Process
Locomotion
Metabolic Process
Rhythmic Process
Signaling
Single-Organism Process
Growth
Uncategorized

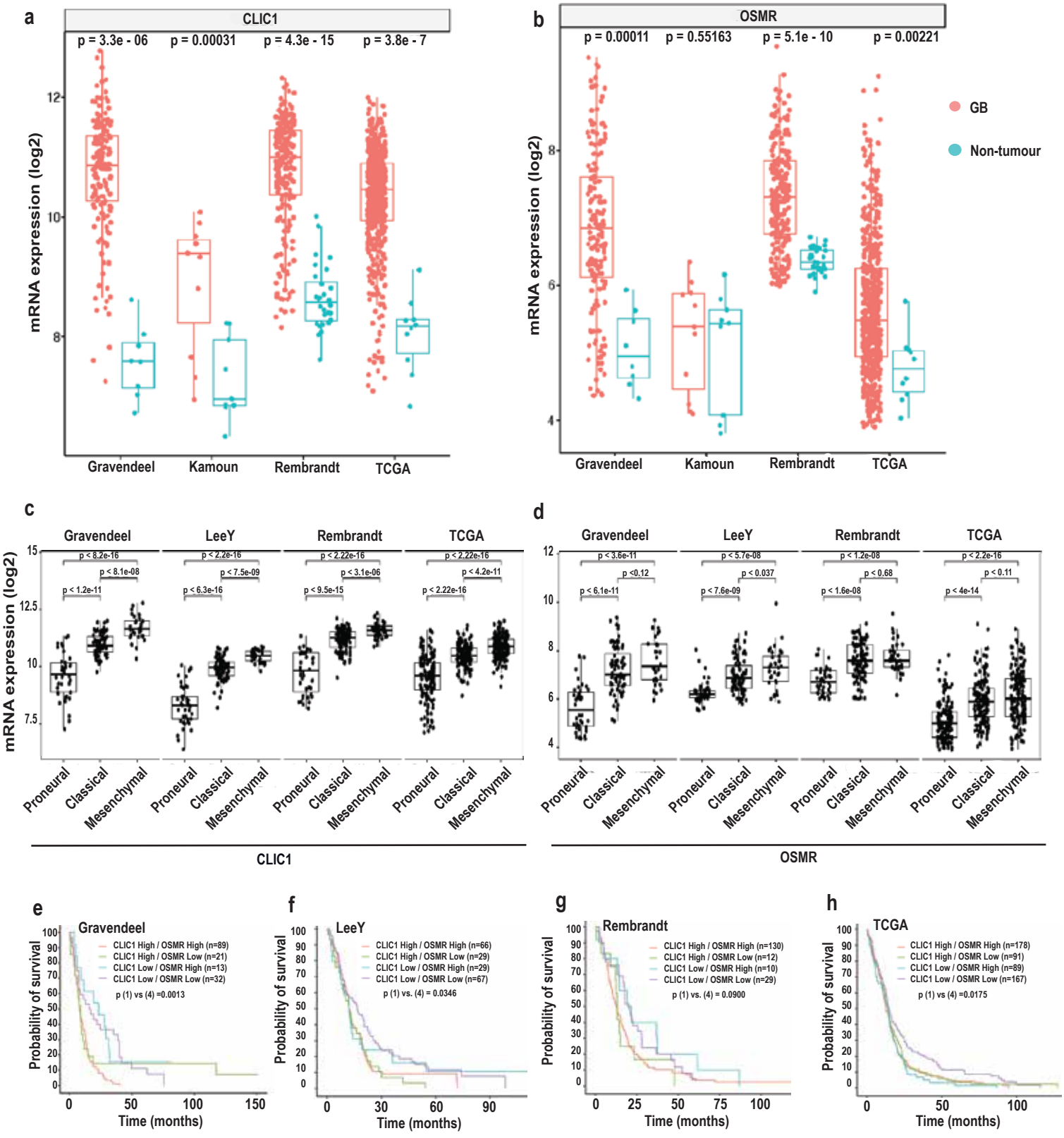
a
CLIC1
p = 3.3e - 06
p = 0.00031
p = 4.3e - 15
p = 3.8e - 7
mRNA expression (log2)
Gravendeel
Kamoun
Rembrandt
TCGA
b
OSMR
p = 0.00011
p = 0.55163
p = 5.1e - 10
p = 0.00221
GB
Non-tumour
c
d
Proneural
Classical
Mesenchymal
CLIC1
OSMR
e
Gravendeel
CLIC1 High / OSMR High (n=89)
CLIC1 High / OSMR Low (n=21)
CLIC1 Low / OSMR High (n=13)
CLIC1 Low / OSMR Low (n=32)
p (1) vs (4) =0.0013
f
LeeY
CLIC1 High / OSMR High (n=66)
CLIC1 High / OSMR Low (n=29)
CLIC1 Low / OSMR High (n=29)
CLIC1 Low / OSMR Low (n=67)
p (1) vs. (4) = 0.0346
g
Rembrandt
CLIC1 High / OSMR High (n=130)
CLIC1 High / OSMR Low (n=12)
CLIC1 Low / OSMR High (n=10)
CLIC1 Low / OSMR Low (n=29)
p (1) vs. (4) = 0.0900
h
TCGA
CLIC1 High / OSMR High (n=178)
CLIC1 High / OSMR Low (n=91)
CLIC1 Low / OSMR High (n=89)
CLIC1 Low / OSMR Low (n=167)
p (1) vs (4) =0.0175
Probability of survival
Time (months)

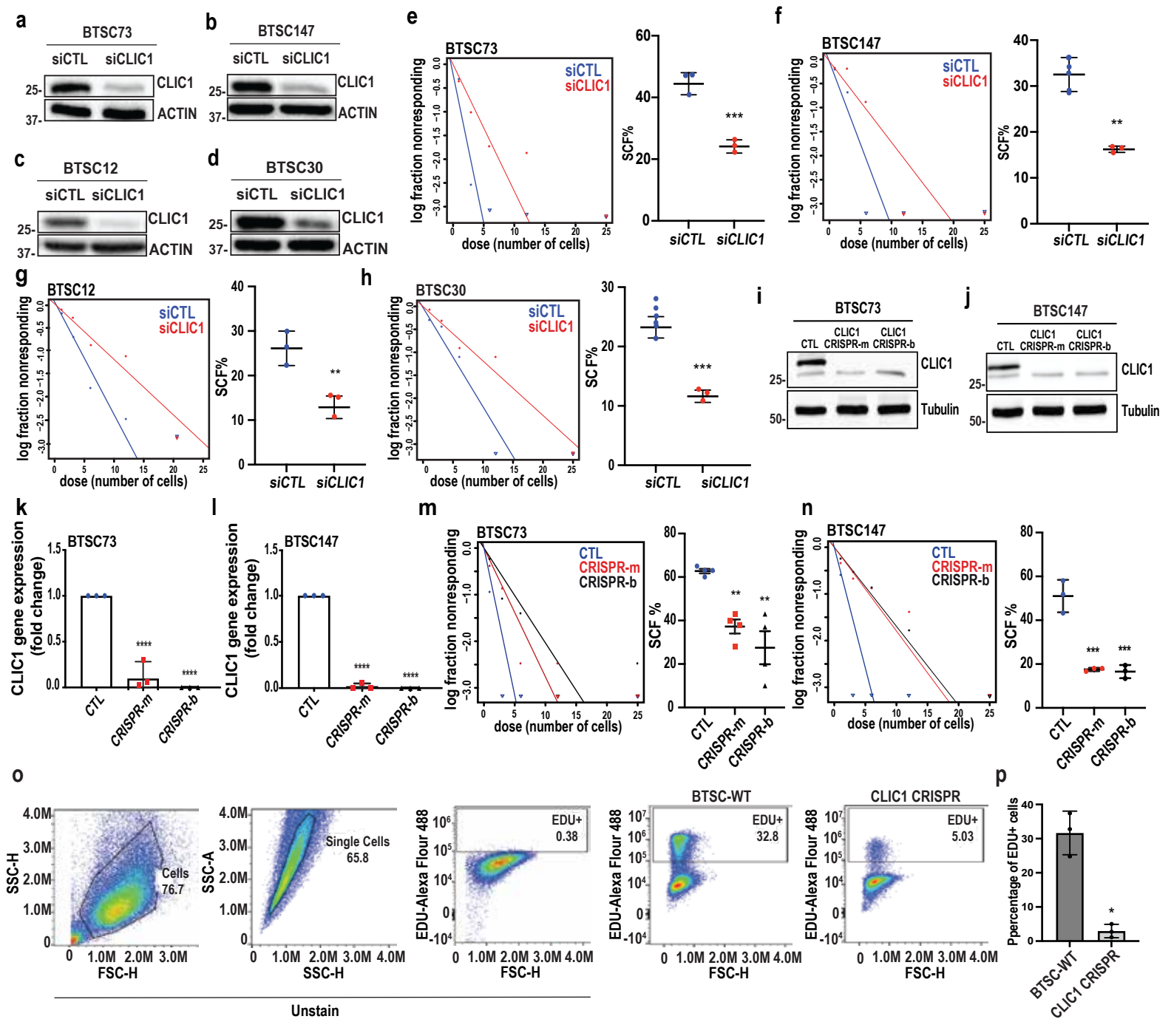
a
BTSC73
siCTL siCLIC1
25-
37-
CLIC1
ACTIN
b
BTSC147
siCTL siCLIC1
25-
37-
CLIC1
ACTIN
c
BTSC12
siCTL siCLIC1
25-
37-
CLIC1
ACTIN
d
BTSC30
siCTL siCLIC1
25-
37-
CLIC1
ACTIN
e
BTSC73
siCTL
siCLIC1
log fraction nonresponding
dose (number of cells)
SCF%
***
siCTL siCLIC1
f
BTSC147
siCTL
siCLIC1
log fraction nonresponding
dose (number of cells)
SCF%
**
siCTL siCLIC1
g
BTSC12
siCTL
siCLIC1
log fraction nonresponding
dose (number of cells)
SCF%
**
siCTL siCLIC1
h
BTSC30
siCTL
siCLIC1
log fraction nonresponding
dose (number of cells)
SCF%
***
siCTL siCLIC1
i
BTSC73
CTL CLIC1 CRISPR-m CLIC1 CRISPR-b
25-
50-
CLIC1
Tubulin
j
BTSC147
CTL CLIC1 CRISPR-m CLIC1 CRISPR-b
25-
50-
CLIC1
Tubulin
k
BTSC73
CLIC1 gene expression (fold change)
****
****
CTL CRISPR-m CRISPR-b
l
BTSC147
CLIC1 gene expression (fold change)
****
****
CTL CRISPR-m CRISPR-b
m
BTSC73
CTL
CRISPR-m
CRISPR-b
log fraction nonresponding
dose (number of cells)
SCF %
**
**
CTL CRISPR-m CRISPR-b
n
BTSC147
CTL
CRISPR-m
CRISPR-b
log fraction nonresponding
dose (number of cells)
SCF %
***
***
CTL CRISPR-m CRISPR-b
o
SSC-H
FSC-H
Cells
76.7
SSC-A
SSC-H
Single Cells
65.8
EDU-Alexa Flour 488
FSC-H
EDU+
0.38
BTSC-WT
EDU-Alexa Flour 488
FSC-H
EDU+
32.8
CLIC1 CRISPR
EDU-Alexa Flour 488
FSC-H
EDU+
5.03
Unstain
p
Ppercentage of EDU+ cells
*
BTSC-WT
CLIC1 CRISPR

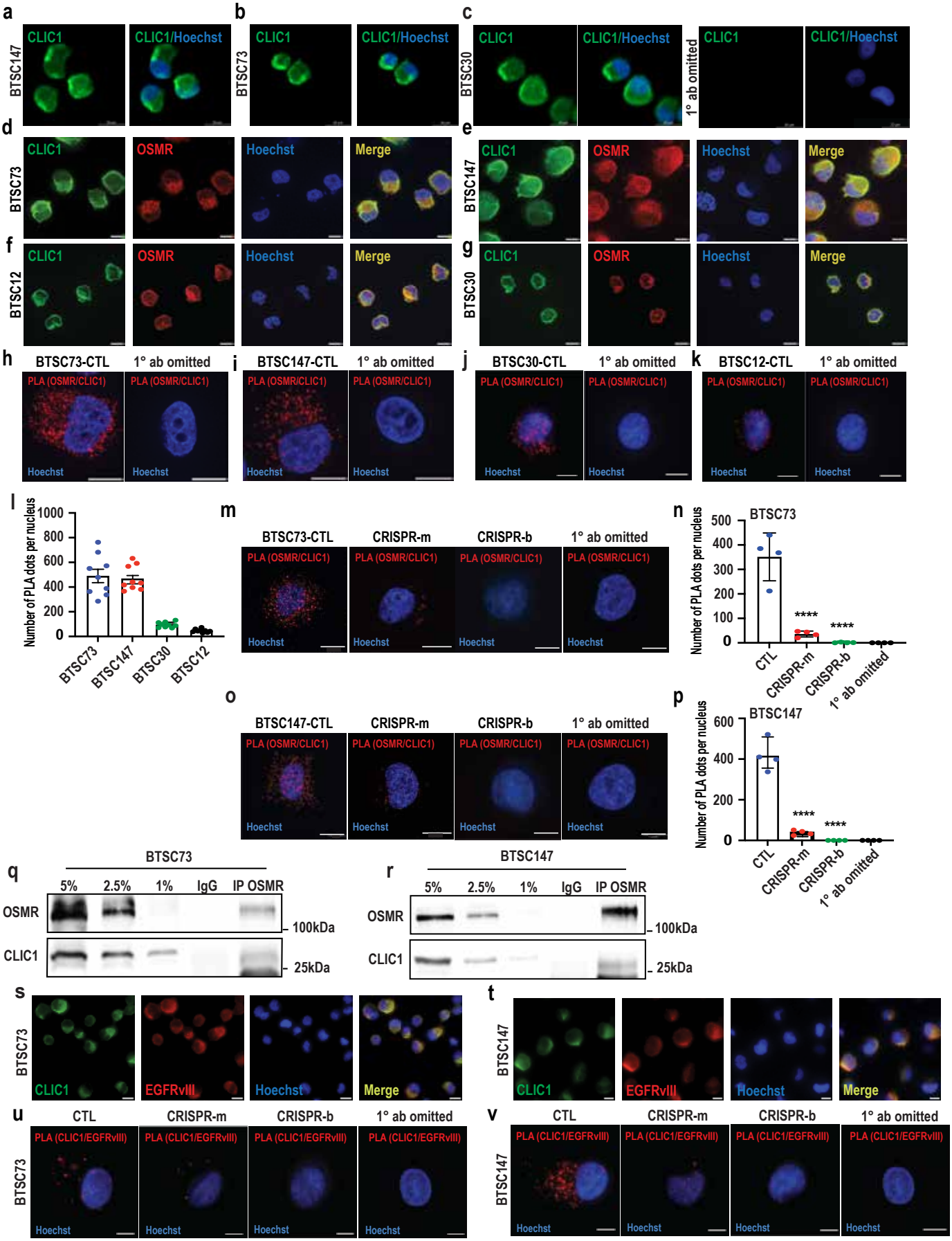
a
BTSC147
CLIC1
CLIC1/Hoechst
b
BTSC73
CLIC1
CLIC1/Hoechst
c
BTSC30
CLIC1
CLIC1/Hoechst
1° ab omitted
CLIC1
CLIC1/Hoechst
d
BTSC73
CLIC1
OSMR
Hoechst
Merge
e
BTSC147
CLIC1
OSMR
Hoechst
Merge
f
BTSC12
CLIC1
OSMR
Hoechst
Merge
g
BTSC30
CLIC1
OSMR
Hoechst
Merge
h
BTSC73-CTL
1° ab omitted
PLA (OSMR/CLIC1)
Hoechst
i
BTSC147-CTL
1° ab omitted
PLA (OSMR/CLIC1)
Hoechst
j
BTSC30-CTL
1° ab omitted
PLA (OSMR/CLIC1)
Hoechst
k
BTSC12-CTL
1° ab omitted
PLA (OSMR/CLIC1)
Hoechst
l
Number of PLA dots per nucleus
1000
800
600
400
200
0
BTSC73
BTSC147
BTSC30
BTSC12
m
BTSC73-CTL
CRISPR-m
CRISPR-b
1° ab omitted
PLA (OSMR/CLIC1)
Hoechst
n
BTSC73
Number of PLA dots per nucleus
500
400
300
200
100
0
****
****
CTL
CRISPR-m
CRISPR-b
1° ab omitted
o
BTSC147-CTL
CRISPR-m
CRISPR-b
1° ab omitted
PLA (OSMR/CLIC1)
Hoechst
p
BTSC147
Number of PLA dots per nucleus
600
400
200
0
****
****
CTL
CRISPR-m
CRISPR-b
1° ab omitted
q
BTSC73
5%
2.5%
1%
IgG
IP OSMR
OSMR
CLIC1
100kDa
25kDa
r
BTSC147
5%
2.5%
1%
IgG
IP OSMR
OSMR
CLIC1
100kDa
25kDa
s
BTSC73
CLIC1
EGFRvIII
Hoechst
Merge
t
BTSC147
CLIC1
EGFRvIII
Hoechst
Merge
u
BTSC73
CTL
CRISPR-m
CRISPR-b
1° ab omitted
PLA (CLIC1/EGFRvIII)
Hoechst
v
BTSC147
CTL
CRISPR-m
CRISPR-b
1° ab omitted
PLA (CLIC1/EGFRvIII)
Hoechst

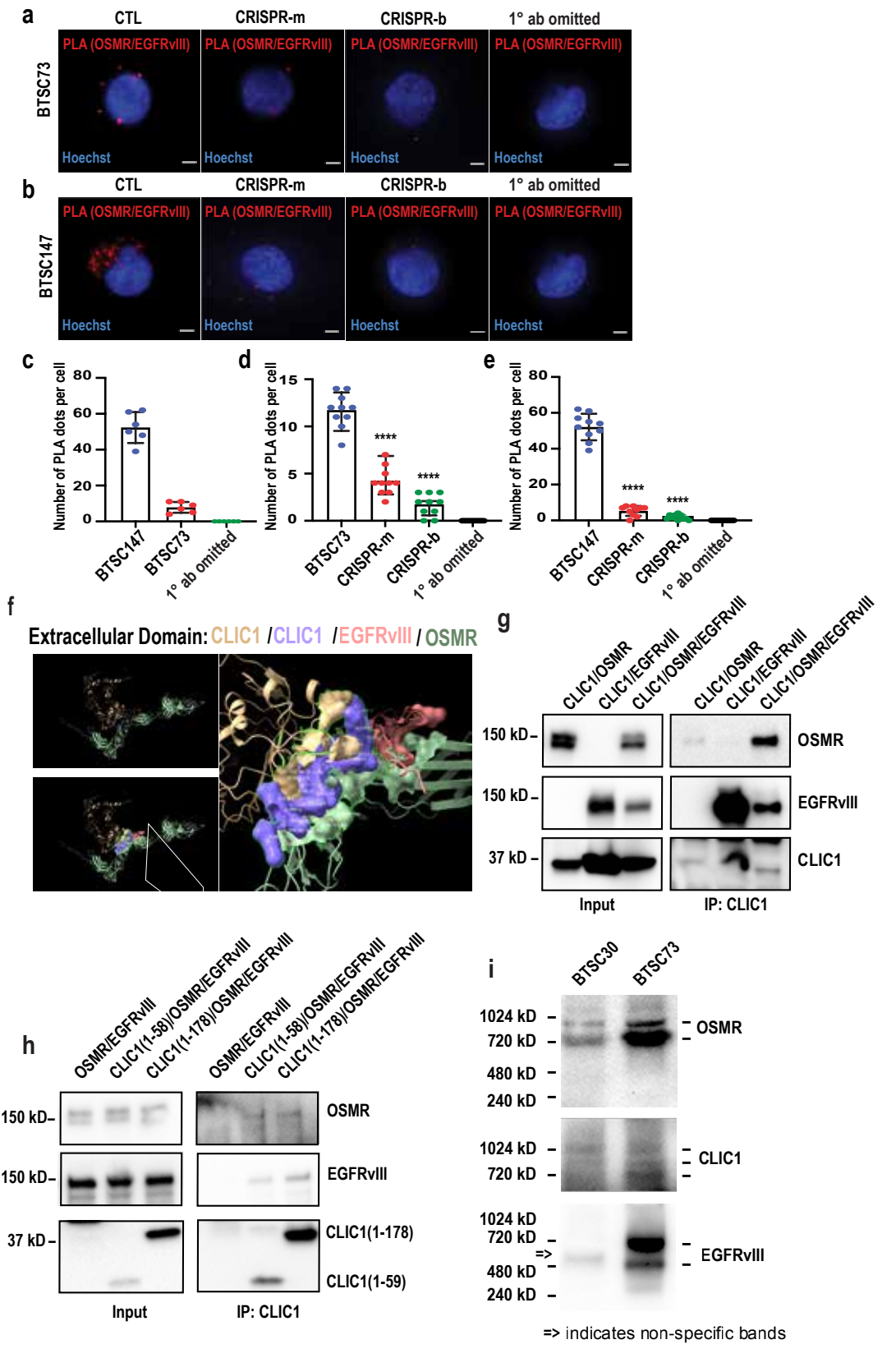
a
CTL
CRISPR-m
CRISPR-b
1° ab omitted
BTSC73
PLA (OSMR/EGFRvIII)
Hoechst
b
BTSC147
c
Number of PLA dots per cell
BTSC147
BTSC73
1° ab omitted
d
BTSC73
CRISPR-m
CRISPR-b
****
e
f
Extracellular Domain: CLIC1 /CLIC1 /EGFRvIII / OSMR
g
CLIC1/OSMR
CLIC1/EGFRvIII
CLIC1/OSMR/EGFRvIII
150 kD
37 kD
OSMR
EGFRvIII
CLIC1
Input
IP: CLIC1
h
OSMR/EGFRvIII
CLIC1(1-58)/OSMR/EGFRvIII
CLIC1(1-178)/OSMR/EGFRvIII
CLIC1(1-178)
CLIC1(1-59)
i
BTSC30
BTSC73
1024 kD
720 kD
480 kD
240 kD
=> indicates non-specific bands

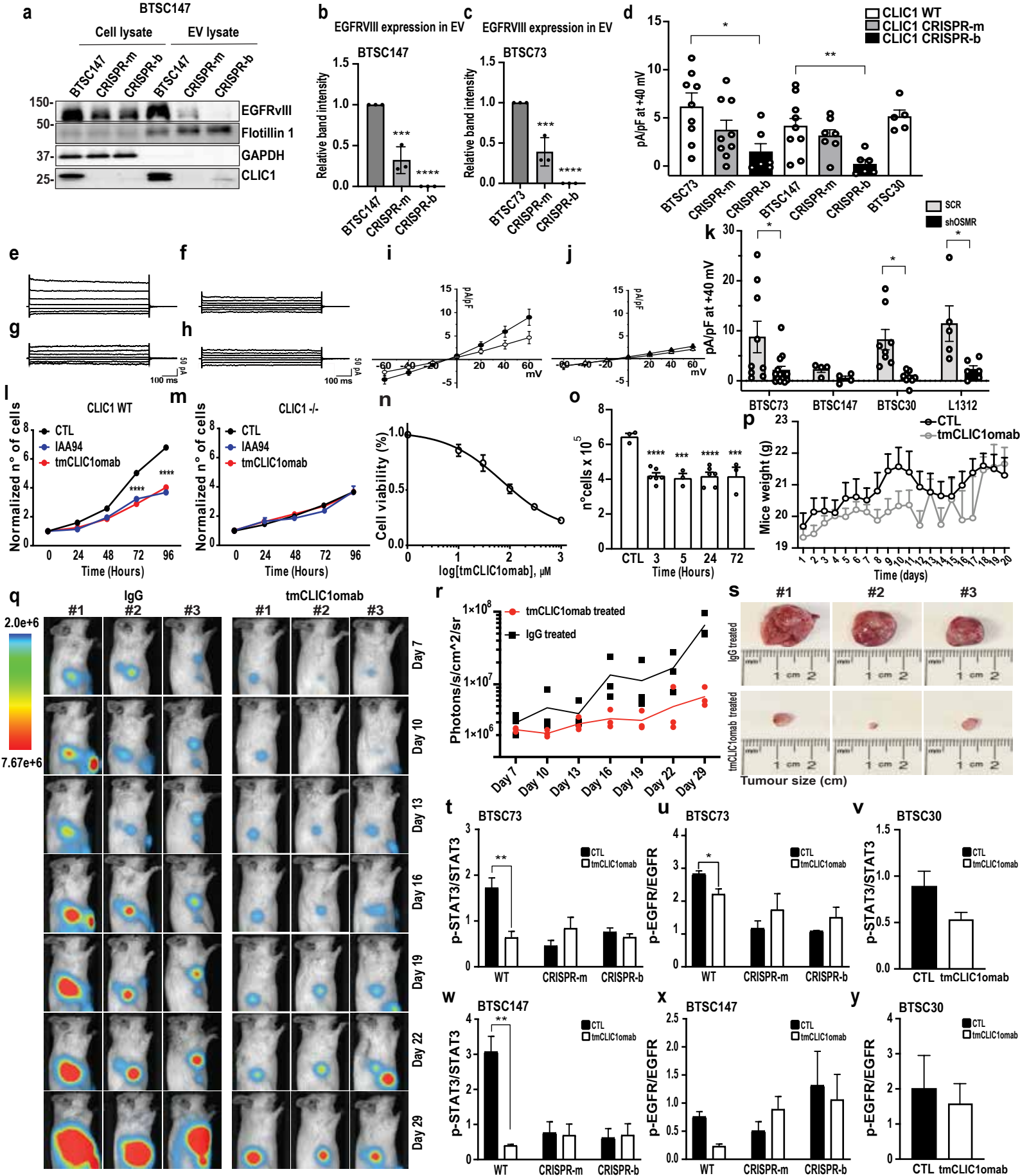
a
BTSC147
Cell lysate
EV lysate
BTSC147
CRISPR-m
CRISPR-b
BTSC147
CRISPR-m
CRISPR-b
150-
50-
37-
25-
EGFRvIII
Flotillin 1
GAPDH
CLIC1
b
EGFRVIII expression in EV
BTSC147
Relative band intensity
BTSC147
CRISPR-m
CRISPR-b
c
EGFRVIII expression in EV
BTSC73
Relative band intensity
BTSC73
CRISPR-m
CRISPR-b
d
CLIC1 WT
CLIC1 CRISPR-m
CLIC1 CRISPR-b
pA/pF at +40 mV
BTSC73
CRISPR-m
CRISPR-b
BTSC147
CRISPR-m
CRISPR-b
BTSC30
e
f
g
100 ms
50 pA
h
100 ms
50 pA
i
pA/pF
mV
j
pA/pF
mV
k
SCR
shOSMR
pA/pF at +40 mV
BTSC73
BTSC147
BTSC30
L1312
l
CLIC1 WT
Normalized n° of cells
CTL
IAA94
tmCLIC1omab
Time (Hours)
m
CLIC1 -/-
Normalized n° of cells
CTL
IAA94
tmCLIC1omab
Time (Hours)
n
Cell viability (%)
log[tmCLIC1omab], μM
o
n°cells x 10^5
CTL
3
5
24
72
Time (Hours)
p
CTL
tmCLIC1omab
Mice weight (g)
Time (days)
q
IgG
tmCLIC1omab
#1
#2
#3
2.0e+6
7.67e+6
Day 7
Day 10
Day 13
Day 16
Day 19
Day 22
Day 29
r
tmCLIC1omab treated
IgG treated
Photons/s/cm^2/sr
Day 7
Day 10
Day 13
Day 16
Day 19
Day 22
Day 29
s
#1
#2
#3
IgG treated
tmCLIC1omab treated
Tumour size (cm)
t
BTSC73
p-STAT3/STAT3
CTL
tmCLIC1omab
WT
CRISPR-m
CRISPR-b
u
BTSC73
p-EGFR/EGFR
CTL
tmCLIC1omab
WT
CRISPR-m
CRISPR-b
v
BTSC30
p-STAT3/STAT3
CTL
tmCLIC1omab
CTL
tmCLIC1omab
w
BTSC147
p-STAT3/STAT3
CTL
tmCLIC1omab
WT
CRISPR-m
CRISPR-b
x
BTSC147
p-EGFR/EGFR
CTL
tmCLIC1omab
WT
CRISPR-m
CRISPR-b
y
BTSC30
p-EGFR/EGFR
CTL
tmCLIC1omab
CTL
tmCLIC1omab

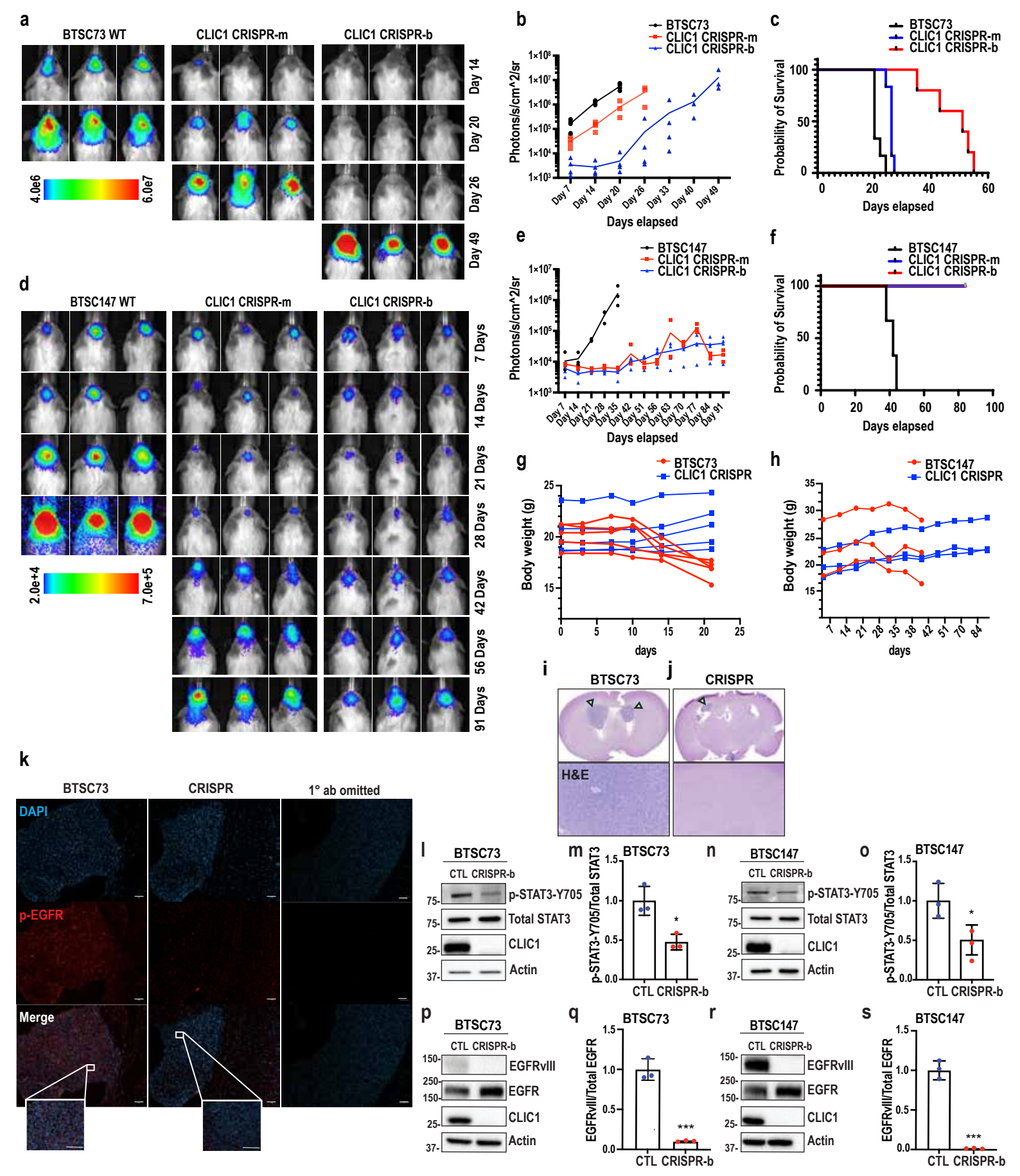
a
BTSC73 WT
CLIC1 CRISPR-m
CLIC1 CRISPR-b
Day 14
Day 20
Day 26
Day 49
4.0e6
6.0e7
b
BTSC73
CLIC1 CRISPR-m
CLIC1 CRISPR-b
Photons/s/cm^2/sr
Days elapsed
c
BTSC73
CLIC1 CRISPR-m
CLIC1 CRISPR-b
Probability of Survival
Days elapsed
d
BTSC147 WT
CLIC1 CRISPR-m
CLIC1 CRISPR-b
7 Days
14 Days
21 Days
28 Days
42 Days
56 Days
91 Days
2.0e+4
7.0e+5
e
BTSC147
CLIC1 CRISPR-m
CLIC1 CRISPR-b
Photons/s/cm^2/sr
Days elapsed
f
BTSC147
CLIC1 CRISPR-m
CLIC1 CRISPR-b
Probability of Survival
Days elapsed
g
BTSC73
CLIC1 CRISPR
Body weight (g)
days
h
BTSC147
CLIC1 CRISPR
Body weight (g)
days
i
BTSC73
j
CRISPR
H&E
k
BTSC73
CRISPR
1° ab omitted
DAPI
p-EGFR
Merge
l
BTSC73
CTL CRISPR-b
p-STAT3-Y705
Total STAT3
CLIC1
Actin
m
BTSC73
p-STAT3-Y705/Total STAT3
CTL CRISPR-b
n
BTSC147
CTL CRISPR-b
p-STAT3-Y705
Total STAT3
CLIC1
Actin
o
BTSC147
p-STAT3-Y705/Total STAT3
CTL CRISPR-b
p
BTSC73
CTL CRISPR-b
EGFRvIII
EGFR
CLIC1
Actin
q
BTSC73
EGFRvIII/Total EGFR
CTL CRISPR-b
r
BTSC147
CTL CRISPR-b
EGFRvIII
EGFR
CLIC1
Actin
s
BTSC147
EGFRvIII/Total EGFR
CTL CRISPR-b